Cerebral Cortex, 2018; 1–18

doi: 10.1093/cercor/bhy025
Original Article

ORIGINAL ARTICLE

Neural Representations of the Full Spatial Field in Auditory Cortex of Awake Marmoset (*Callithrix jacchus*)

Evan D. Remington and Xiaoqin Wang

Department of Biomedical Engineering, Johns Hopkins University School of Medicine, Baltimore, MD 21025, USA

Address correspondence to Xiaoqin Wang, Ph.D., Department of Biomedical Engineering, Johns Hopkins University School of Medicine, 720 Rutland Ave., Traylor 410, Baltimore, MD 21025, USA. Email: xiaoqin.wang@jhu.edu

Abstract

Unlike visual signals, sound can reach the ears from any direction, and the ability to localize sounds from all directions is essential for survival in a natural environment. Previous studies have largely focused on the space in front of a subject that is also covered by vision and were often limited to measuring spatial tuning along the horizontal (azimuth) plane. As a result, we know relatively little about how the auditory cortex responds to sounds coming from spatial locations outside the frontal space where visual information is unavailable. By mapping single-neuron responses to the full spatial field in awake marmoset (*Callithrix jacchus*), an arboreal animal for which spatial processing is vital in its natural habitat, we show that spatial receptive fields in several auditory areas cover all spatial locations. Several complementary measures of spatial tuning showed that neurons were tuned to both frontal space and rear space (outside the coverage of vision), as well as the space above and below the horizontal plane. Together, these findings provide valuable new insights into the representation of all spatial locations by primate auditory cortex.

Key words: auditory cortex, marmoset, spatial representation

Introduction

For both humans and other animals, the ability to localize sound sources provides biologically important information about objects and events. Unlike visual signals, sound can reach the sensory epithelia and be localized behaviorally from any direction. Auditory cortex is essential for many behaviors involving sound localization (Jenkins and Masterton 1982; Bizley et al. 2007; Lomber and Malhotra 2008). While spatial coding studies in the past have generated considerable knowledge, how the auditory cortex represents the location of sound sources at the level of single and populations of neurons remains an unsettled question. Most previous studies investigating the representation of sound location in auditory cortex have measured responses to individual sounds delivered in free field along a single dimension of azimuth (Rajan et al. 1990; Middlebrooks et al. 1994; Furukawa and Middlebrooks 2002; Stecker et al. 2003; Woods et al. 2006; King et al. 2007; Werner-Reiss and Groh 2008; Lee and Middlebrooks 2013; Yao et al. 2013), or elevation (Xu et al. 1998; Stecker et al. 2003), or over a limited portion of frontal space (Recanzone et al. 2000; Zhou and Wang 2012; Razak et al. 2015) that is also covered by vision. Except in a few studies where virtual acoustic space stimuli were used to probe the full spatial field (Brugge et al. 1994, 1996; Schnupp et al. 2001; Mrsic-Flogel et al. 2005), there have been no systematic evaluations of responses to the full special field at the level of single neurons in auditory cortex, and none have been conducted in awake animals. To understand the nature of spatial representation in the auditory system, it is crucial to measure how single neurons in auditory cortex represent the full spatial field both within and outside the coverage of vision. This is the objective of the present study.

The few studies investigating cortical responses to a full spatial field have been conducted using anesthetized animals

(Middlebrooks and Pettigrew 1981; Brugge et al. 1994, 1996; Schnupp et al. 2001; Mrsic-Flogel et al. 2005). Many studies in anesthetized animals report a predominance of broad spatial receptive fields centered at extreme contralateral locations, which generally increase in size as sound level increases (Middlebrooks and Pettigrew 1981; Middlebrooks et al. 1994; Brugge et al. 1996; Middlebrooks and Xu 1998; Xu et al. 1998; Stecker et al. 2003; Mrsic-Flogel et al. 2005). However, more recent studies of azimuth (Mickey and Middlebrooks 2003; Woods et al. 2006; Lee and Middlebrooks 2013) and frontal field tuning (Zhou and Wang 2012) in awake animals have reported neurons with preferred locations more evenly distributed throughout tested locations, responses to restricted spatial locations, and receptive fields that on average do not significantly increase in size as sound level increases. However, it is possible that these studies missed crucial information due to spatial locations not tested. A study of full-field spatial tuning in awake animals is therefore critical to fill the knowledge gap in this area.

The primate auditory cortex contains multiple anatomically defined areas (Kaas and Hackett 1998; Rauschecker 1998; Hackett 2011). It has been shown that caudal areas are more selective to spatial location than rostral areas (Rauschecker and Tian 2000; Tian et al. 2001; Woods et al. 2006). Because these studies were based on partial sampling of space, it is important to examine the notion of increased spatial selectivity using full-field spatial receptive fields in both caudal and rostral areas. We addressed this limitation in the present study by measuring responses of single neurons in primary auditory cortex (A1), the rostral fields (R/RT), and the caudal belt areas (CM/CL) of awake marmoset monkeys to broad-band sounds presented from the free field across the full spatial field. Our findings suggest that primate auditory cortex represents the entire space around a subject by a distributed network of spatially tuned neurons.

Materials and Methods

Animal Preparation and Electrophysiological Procedures

A single-electrode recording preparation (Lu et al. 2001) was used to record single-neuron activity in the auditory cortex (left hemisphere) of three awake female common marmoset monkeys (*Callithrix jacchus*). All subjects were trained to sit in a custom-designed primate chair and perform a behavioral task (Remington et al. 2012) for a separate study. After 1–2 months of behavioral training, two stainless steel headposts were attached to the skull under sterile conditions with the animal deeply anesthetized by isoflurane (0.5–2.0%, mixed with 50% O_2 and 50% nitrous oxide). The headposts served to maintain a stable head orientation of the subject during electrophysiological recordings; however in this study, only one (the front) headpost was used for head fixation. To access auditory cortex, small craniotomies (1.0–1.1 mm in diameter) were made in the skull over the superior temporal gyrus to allow for the penetration of electrodes (tungsten electrodes, 2- to 5-MΩ impedance, A-M Systems) via a hydraulic microdrive (Trent-Wells). Single-unit spiking activity, recorded in daily experimental sessions, was sorted online using a template-based spike-sorting program (MSD; Alpha Omega Engineering) and analyzed using custom programs written in Matlab (Mathworks). An infrared video camera was used to monitor the state of subjects throughout recording sessions. Experimental procedures were approved by the Institutional Animal Care and Use Committee of the Johns Hopkins University following National Institutes of Health guidelines.

Experimental Setup

Experiments were conducted in a double-walled sound-proof chamber (Industrial Acoustics, IAC) with the internal walls, ceiling, and floor lined with ~3 in. acoustic absorption foam (Sonex). Acoustic stimuli were delivered using an array of 24 speakers (FT28D, Dome Tweeter, Fostex) covering a complete sphere (Fig. 1). The loudspeakers were mounted at a distance of 1 m to the animal's head and covered five elevations (ELs) at 45° spacing and several azimuths (AZs). One speaker was located directly above the animal, seven speakers each were evenly spaced at ±45° EL (AZ at −45° EL: ±25.7°, ±77.1°, ±128.6°, and 180°; AZ at 45° EL: 0°, ±51.4°, ±102.9°, and ±154.3°), eight speakers were evenly positioned at 0° EL (AZ: 0°, ±45°, ±90°, ±135°, and 180°), and finally one speaker was located at either −85° EL (for subject 1) or −67.5° EL at 0° AZ. Subjects sat in a wire mesh primate chair mounted

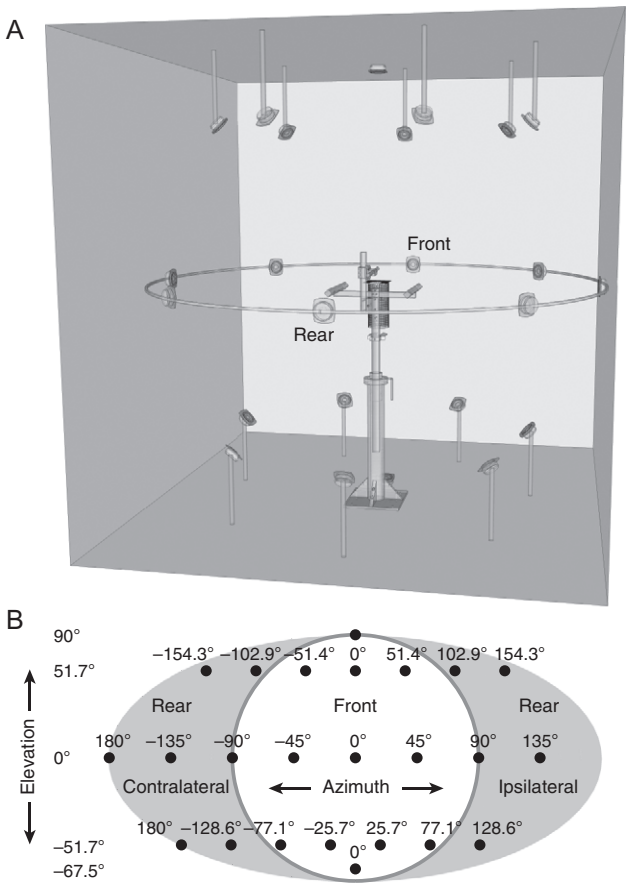

Figure 1. Full-field speaker layout. (A) 3D model of sound-proof chamber with 24-speaker array, and marmoset chair. This experimental configuration was designed to allow sound delivery from all directions. Speakers were positioned 1 m from the center of the chamber at multiple elevations (EL) and azimuth (AZ) locations. One speaker was located directly above the animal, seven speakers each were evenly spaced at ± 45° EL (AZ at −45° EL: ±25.7°, ±77.1°, ±128.6°, and 180°; AZ at 45° EL: 0°, ±51.4°, ±102.9°, and ±154.3°), eight speakers were evenly positioned at 0° EL (AZ: 0°, ±45°, ±90°, ±135°, and 180°), and finally one speaker was located at either −85° EL (for subject 1) or −67.5° EL at 0° AZ. (B) A Fournier projection of space, opened at the rear meridian, viewed from the front. Speaker locations are indicated by black circles and are labeled with azimuth and elevation values above each location and to the left of the projection, respectively. This projection is used to illustrate spatial receptive fields in the manuscript. As recordings were made in the left hemispheres of all subjects, left (positive azimuth values; figure perspective is facing backward at the front of the array) and right (negative azimuth values) hemifields represent ipsilateral and contralateral space, respectively.

onto a single stainless steel bar such that the animal's head was centered in the room, facing the speaker at 0° AZ & EL. Consistent head pitch was achieved across animals through consistent positioning of the headposts across animals. All positive azimuth angles correspond to speakers ipsilateral to the recording site or to an ipsilateral shift if changes in azimuth were analyzed. Because all recordings were made from the left hemisphere, this meant that positive azimuth angles also corresponded to the left spatial hemifield. During experiments, eye position was not controlled.

Acoustic Stimuli

Stimuli were generated in Matlab at a sampling rate of 97.7 kHz using custom software. Digital signals were converted to analog (RX6, 2 channels D/A; Tucker-Davis Technologies), then analog signals were attenuated (PA5 x2; Tucker-Davis Technologies), power amplified (Crown Audio x2), and played through a chosen channel of a power multiplexer (PM2R x2, 16 channels; Tucker-Davis Technologies). The amplifiers were adjusted so that the stimulus intensity of a 4 kHz tone from the front speaker was 95 decibels of sound pressure level (dB SPL) at 0 dB attenuation measured with a 0.5 in. free-field microphone (Brüel & Kjær model 4191) at the location where the animal's head would be. Loudspeaker responses were measured using Golay codes (Zhou et al. 1992) and had a relatively flat frequency response curve (±3–7 dB) and minimal spectral variation across speakers (<7 dB re mean) across the range of frequencies of the stimuli used; the largest (5–7 dB) spectral deviations occurred in narrow bandwidths near the upper limit of speakers' frequency range (above 28 kHz), above the first spectral notch measured in marmoset head-related transfer functions (Slee and Young 2010). All intensities in this report are expressed in terms of the peak-to-peak pure tone equivalent dB SPL.

When possible, neurons were characterized for frequency, intensity, and spatial tuning. Characterization was performed by recording responses to sets of stimuli that were typically 200 ms in length, presented in pseudorandom order. Each stimulus was delivered between 5 and 10 times, with an interstimulus interval of 600 ms. For frequency tuning, stimuli consisted of pure tones, band-pass–filtered Gaussian noise, random spectral shape (RSS) stimuli (Yu and Young 2000; Barbour and Wang 2003), and occasionally frequency-modulated (FM) sweeps. The frequency axis was sampled in 0.1 octave steps, typically over a four octave range (2–32 kHz). All firing rates were calculated over a time window beginning 15 ms after stimulus onset and 20 ms after stimulus offset; "offset" responses (occurring >20 ms post stimulus) were not analyzed. Best frequency (BF) was defined as the frequency that led to the maximum evoked significant firing rate, or for neurons only driven by RSS stimuli, the highest calculated linear RSS weight (in spikes/dB/second; see Yu and Young 2000). For spatial tuning, stimuli comprised band-pass–filtered unfrozen Gaussian noise, single RSS stimulus tokens, and occasionally FM sweeps. All stimuli used to measure spatial receptive fields were either band-pass filtered or constructed to have energy between 2 and 32 kHz.

Characterization of Spatial Receptive Fields

To partially alleviate biases in calculated tuning properties that could be introduced by uneven spacing of speakers, spatial receptive fields were generated by interpolating responses to the 24-speaker array into a 5° × 5° (2592 zone) vertical pole grid according to the spherical distance-weighted mean of the two nearest speaker locations, with the weight at a single interpolated location from speaker i calculated as

$$\text{weight}_i = \frac{(1/\text{distance}_i)^2}{\sum_{j=1}^{2}(1/\text{distance}_j)^2} \quad (1)$$

where distance is the spherical distance between speaker i and the center of the grid zone.

The resulting spatial receptive fields were used to calculate several tuning properties. First,

$$\text{tuning area} = \frac{\sum_{\{i:r_i>\text{thresdhold}\}}\text{area}_i}{\text{total area}} \quad (2)$$

where area_i is the area of grid zone i, r_i is the interpolated firing rate for grid zone i, and "threshold" is classically defined as the half maximal firing rate. Thus, the maximum tuning area is 1, while a response to a single location results in a tuning area of ~0.045. The tuning vector (TV) roughly characterizes neurons' preferred direction as well as receptive field dispersion. It is calculated as follows:

$$\text{tuning vector} = \frac{\sum r_i * \text{vector}_i * \text{area}_i}{\sum r_i * \text{area}_i} \quad (3)$$

where vector_i is the unit vector pointing to the center of grid zone i. The tuning vector comprised three components (x, y, and z), representing contralateral versus ipsilateral (x), front versus back (y), and up versus down (z) preferences. For plotting, the tuning vector was transformed into polar coordinates (i.e., azimuth and elevation). For some directional analyses, tuning vectors were normalized by dividing all components by the tuning vector magnitude, or the norm of the tuning vector. The tuning vector magnitude was also used to assess spatial selectivity. A response to a single location results in a tuning vector magnitude of ~1; responses to additional locations will result in a smaller magnitude down to a minimum of 0. Notably, a neuron responding to only two locations can have a tuning vector magnitude of 0 if the two locations are diametrically opposed and the firing rates are identical.

To confirm the accuracy of the interpolation procedure, we simulated simple 24-speaker–receptive fields centered around randomly sampled tuning vectors and then tested how well the original tuning vectors could be recovered using the interpolated data. For each simulated receptive field, the firing rate at each speaker location was the value of a Gaussian distribution function evaluated at the angle between the vector of the speaker location and the tuning vector defining the receptive field. The x, y, and z components of the tuning vector were uniformly distributed between −1 and 1, while for the Gaussian tuning function, the standard deviation parameter governing the tuning selectivity was gamma distributed with a mean of 60 degrees and a standard deviation of 30 degrees. The difference between the true tuning vector used to generate the rate function and the tuning vector calculated using the interpolated data was small (median = 0.5 degrees, interquartile range (IQR) = 0.4 degrees, n = 1000 simulated spatial receptive fields), indicating that underling tuning vectors can be accurately recovered from the interpolated data.

Spatial receptive fields measured in auditory cortex neurons had one or more contiguous regions, or "peaks," with interpolated firing rates above the half maximal firing rate. We defined a peak as a bounded region of the interpolated receptive field in which firing rates were greater than 50% of the maximum firing rate. These regions were identified using Matlab's "contourc"

function to generate a 50% response contour on a 2D map array and then combining regions at opposite edges of the projection where appropriate. Units were further classified as having multiple peaks in the lateral dimension (contralateral to ipsilateral, ignoring front vs back), along the median plane (elevation and front vs back), or both using non-interpolated rates to the 24-speaker locations. For the lateral dimension, locations were divided into nine groups based on the projection in the contralateral/ipsilateral axis (i.e., −1 to 1), and for the median plane analysis, locations were divided into 12 groups based on the median plane angle. This grouping was to ensure that firing rate differences between speakers with very small differences in the dimension of interest but larger differences in the orthogonal dimension did not lead to a spurious identification of peaks. For example, the speakers at AZ −45° EL 0° and AZ −51.7° EL 45° were placed in the same laterality group (see Fig. 1). For this analysis, a neuron was considered as having multiple peaks along a dimension of interest if the maximum firing rate of any two groups along that dimension were separated by a trough—a group with a maximum rate that was less than 50% of the lesser of the first two. In the case of the median plane, two such troughs were required as response functions were evaluated on a circle.

If a neuron's spatial receptive field was measured with more than one stimulus type or sound level, the "best" receptive field with the single highest trial-averaged firing rate over all stimulus sets (i.e., the neuron's preferred stimulus) was used. Neurons were included in analyses if they responded with a significantly elevated firing rate relative to the spontaneous rate to one or more locations ($P < 0.001$, Wilcoxon rank-sum test and average firing rate of at least one spike per stimulus). For all statistical tests performed on all three cortical areas or all pairs of areas, significance was evaluated against Bonferroni-corrected significance level of $\alpha = 0.05/3 = 0.0167$. All correlation values are Spearman's r.

Principal Component Analysis, Clustering, and Euclidean Distance

The following population-level analyses were performed using best receptive fields normalized by the maximum firing rate across locations for the best stimulus.

In order to quantify the variability in spatial receptive field shapes, principal component analysis (PCA) was performed to identify the orthogonal dimensions along which receptive fields varied most strongly across neurons. For this analysis, the $n \times 24$ (n = number of neurons; 24 speakers) dimensional vector of normalized spatial receptive fields was analyzed with Matlab's "princomp" function to generate the 24 principal components of the centered data, ordered by the variance of the original dataset captured by each component.

The principal component scores for the first five principal component dimensions, as well as the full 24D data, were then used to attempt to cluster the data using a k-means clustering algorithm available in Matlab. This is an unsupervised clustering algorithm and will cluster data regardless of the existence of true clusters. To test for evidence for the existence of clusters within the data, the gap statistic (Tibshirani et al. 2001) was measured on the results of the k-means clustering algorithm for each number of clusters. First, let

$$W_k = \sum_{r=1}^{k} \frac{1}{2n_r} D_r \tag{4}$$

with D_r representing the sum of all pairwise distances (here squared Euclidean) in cluster r. W_k is a measure of dispersion pooled across clusters. The gap statistic is then calculated as

$$\mathrm{Gap}_n(k) = E_n\{\log(W_k)\} - \log(W_k) \tag{5}$$

where n is the number of samples in the population, k is the number of clusters imposed on the dataset, and $E\{\log(W_k)\}$ is the expectation of W_k with a sample of size n using an appropriate reference distribution. The goal is to maximize the "gap" between the reference W_k and the actual W_k by correctly choosing k, the number of clusters. The reference distribution was a scaled multivariate uniform distribution. Here, the k-means and gap statistic analyses were performed using Matlab's Statistics and Machine Learning Toolbox.

To estimate the ability of the neural populations to discriminate between the tested sound source locations, we calculated the Euclidean distances between the N-neuron response vectors for each pair of locations, normalized by the number of neurons in the population.

$$\vec{d}_{i,j} = \sqrt{\frac{1}{N} \sum_n (r_i^n - r_j^n)^2} \tag{6}$$

where r_i^n and r_j^n are the averaged responses of neuron n to locations i and j for a constant stimulus type and intensity. For each speaker location, the Euclidean distances to the four closest locations (in terms of population response) were averaged as a measure of response uniqueness for that location.

$$d_i = \frac{1}{4} \sum_{j=\min(d_{i,j})}^{4} d_{i,j} \tag{7}$$

Identification of A1, the Rostral Fields R/RT, and Caudal Areas CM/CL

In this study, we recorded neurons from several areas, including A1 (primary auditory cortex), the rostral areas R (for rostral) and RT (for rostrotemporal), and the caudal belt areas CL (caudolateral) and CM (caudomedial). In the marmoset, similar to other nonhuman primate species, A1 is situated largely ventral to the lateral sulcus on the superior temporal plane and exhibits a low-to-high topographical frequency gradient along the rostral–caudal axis. The boundary between A1 and the rostral field R can be identified by a downward to upward frequency gradient reversal along the rostral–caudal axis. Conversely, areas CL and CM can be identified by an abrupt decrease of best frequency at the high-frequency (caudal) border of A1 (Merzenich and Brugge 1973; Aitkin et al. 1986; Kaas and Hackett 2000). In this study, the boundaries between R/RT and A1 and A1 and CM/CL were set by plotting the moving average of best frequency along the rostral–caudal axis, approximately parallel to lateral sulcus, and setting a hard boundary by visual inspection at the local minimum and maximum, respectively, between the two areas (Fig. 2). In this study, we obtained BF from 519 units (measured at a median of 65 dB SPL, IQR = 10 dB). In the two animals for which recordings were made in CM/CL, recordings proceeded caudally until units were no longer driven by auditory stimuli and were sometimes driven by moving visual targets (tested using a laser pointer). Neurons were not separated further into R and RT or CM and CL in this study, and no histological verification was performed. It is possible that a small number of neurons at each boundary were

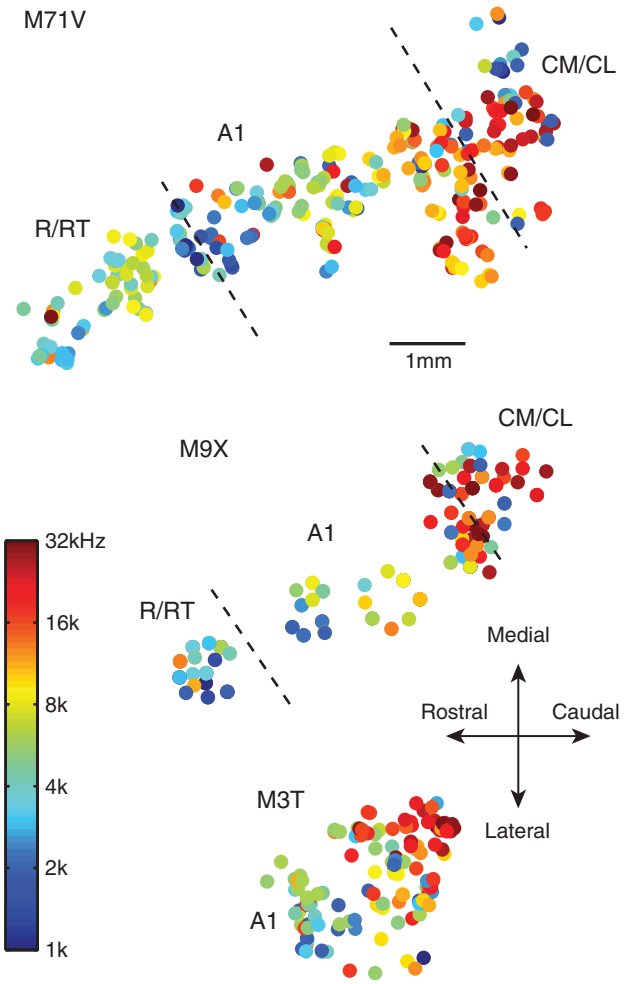

Figure 2. Best-frequency (BF) reversals demarcating areas A1, CM/CL, and R/RT. Dots represent best frequencies of individual neurons recorded auditory cortex. For most neurons, BF refers to the frequency of the pure tone stimulus (or narrow band noise, for non-tone responsive units), which drove a neuron to its highest firing rate. For the remaining neurons, BF was determined using random spectral shape (RSS) stimuli characterization. In two of the three subjects (M71V and M9X), the boundary between A1 and the rostral field R was identified by a downward to upward frequency gradient reversal along the rostral–caudal axis, and areas CL and CM were identified by a decrease in BF at the high-frequency (caudal) border of A1. For illustration, the position of recorded units was jittered slightly in order to visualize multiple units in each recording track.

assigned to the wrong area due to the noisy nature of BF representation in our sample.

Effects of Experimental Acoustics

As mentioned above (see Acoustic Stimuli), there were small differences in spectral output from the different loudspeakers used. We tested whether we could identify an effect of these acoustic differences in neural responses by correlating Euclidean distances between pairs of "points" in neural space and acoustic space associated with each speaker response profile. Neural distances were calculated as described previously (Principal Component Analysis, Clustering, and Euclidean Distance). To generate the points in the space of speaker acoustics, we used the previously measured 79-point power spectra generated from 256-point Hamming-windowed impulse response functions and used the values at frequencies between 2 and 32 kHz to create 24 points in a 79D space. We found no correlation between neural and acoustic Euclidean distances ($r = 0.02$, $P = 0.65$). For comparison, we further measured acoustic response functions from the 24-speaker locations at the ear canals of each subject with small microphones (Knowles Electronics model FG-23329-C05), this time concatenating the 79-point power spectra of each ear to generate 24 points in the 158D binaural acoustic space. Acoustic measurements were taken with and without electrophysiological recording equipment and stereotaxic arms but included the head holder and chair post in both cases. Here, we found significant correlations between acoustic and neural Euclidean distances for each animal tested in both conditions measured (with equipment: $r = 0.58$, $P = 3 \times 10^{-50}$; $r = 0.51$, $P = 2 \times 10^{-37}$; $r = 0.62$, $P = 2 \times 10^{-59}$, without: $r = 0.63$, $P = 2 \times 10^{-62}$; $r = 0.57$, $P = 3 \times 10^{-48}$; $r = 0.59$, $P = 2 \times 10^{-53}$). Together, these results suggest that spatial cues of the head and ears, rather than non-spatial experimental acoustics, were the chief contributors to spatial tuning in the present study.

Results

Single-Neuron Tuning to the Full Spatial Field in Auditory Cortex

We recorded well-isolated single-unit activity in the auditory cortex of three marmoset monkeys while broad-band acoustic stimuli were delivered from one of the 24 speakers placed around an animal (Fig. 1A,B). The speaker array covered both front and rear locations as well as locations above and below the horizontal plane. For the convenience of displaying neural data, we convert left and right speaker locations (relative to an animal) to contralateral and ipsilateral locations (relative to the cortical hemisphere from which a neuron is recorded) (Fig. 1B). We also unfold the front-rear locations onto a plane for display purposes, where frontal space is illustrated by a white circle in Figure 1B and rear space is illustrated by a surrounding gray region. During neural recordings, marmosets sat passively in a wire mesh chair, which was designed to minimize acoustic reflections near the pinna. In total, we recorded spatial receptive fields from 648 single units (408 in A1, 143 in CM/CL, and 97 in R/RT), which responded with a significantly elevated firing rate relative to the spontaneous rate to one or more locations ($P < 0.001$, Wilcoxon rank-sum test and an average of at least one spike per stimulus).

Neurons in marmoset auditory cortex displayed a wide variety of spatial receptive fields when tested across the entire spatial field as illustrated by examples in Figure 3. Figure 3A illustrates raw and spatially interpolated firing rates for an example neuron, which responded to sounds only at the most contralateral locations. At its preferred location, this neuron responded with a burst of spikes following stimulus onset and a sustained response thereafter; away from its preferred location, it fired weakly or not at all. Across the sampled neuron population, spatial receptive fields were centered in contralateral, ipsilateral, lower, upper, front, and rear regions of space (Fig. 3A–E). Among the sampled neurons, 83 (13%) did not meet the criterion to be considered driven by any of the eight azimuth locations at 0° elevation for any combination of stimulus parameters tested (e.g., the unit with spatial receptive field depicted in Fig. 3C), even when a less stringent statistical criterion was used due to the smaller number of speakers ($P < 0.003$).

Spatial receptive fields were quantitatively characterized using metrics that summarized directional preference and spatial selectivity (illustrated in Fig. 3A). Directional preference

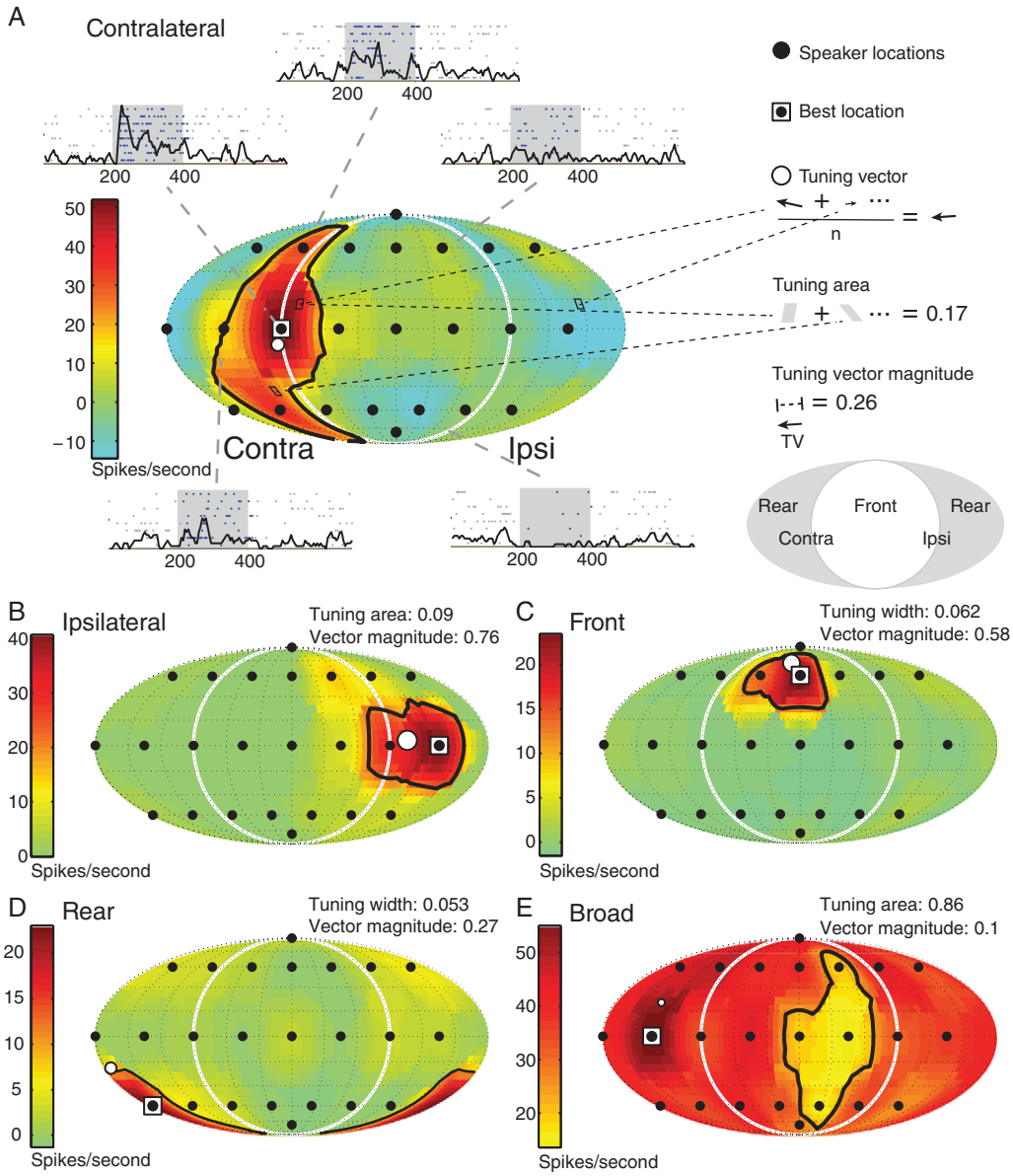

Figure 3. Diversity of spatial receptive fields in auditory cortex. (*A*) Example contralateral tuned spatial receptive field (stimulus: Gaussian noise, 45 dB SPL, A1). Peristimulus time histograms (solid lines) and spike raster plots (dots) show the time course of responses to individual locations. Gray-shaded regions indicate stimulus duration; blue and gray dots represent spikes occurring inside and outside, respectively; a time window that was slightly delayed relative to the stimulus and used to average responses for quantitative analyses. Colored grids show spatially interpolated, spontaneous rate-subtracted mean firing rates. Locations from which sounds suppressed firing below the spontaneous rate are illustrated with negative values. Legend (right), top to bottom: filled circle representing speaker locations; open square designating best location, the speaker that evoked the highest firing rate; open circle designating the tuning vector direction and magnitude (via diameter); schematics for the calculation of tuning vector, tuning area, and tuning vector using interpolated firing rates, along with their values for the illustrated receptive field; key illustrating layout of the 2D spatial projection, as in Figure 1*B*. For tuning vector calculation, arrows represent vectors with direction defined by the location of each grid zone and magnitude equal to the product of the area of each grid zone and average firing rate at that location. Tuning area was the sum of the areas of grid zones (gray rectangles) with raw interpolated firing rates above half the maximum firing rate. The tuning vector (TV) magnitude was the length of the tuning vector. See Materials and Methods for full description of spatial interpolation and other analyses. (*B*) A narrowly tuned, ipsilateral preferring neuron (RSS, 54 dB SPL, A1). (*C*) A narrowly tuned, front/up-preferring neuron (noise, 45 dB SPL, A1). (*D*) A rear/down-preferring neuron (noise, 45 dB SPL, CM/CL). (*E*) A broadly tuned neuron (noise, 45 dB SPL, A1).

was quantified using two complementary metrics: first, the best location was the location that elicited the maximum average firing rate across the 24-speaker array. Second, the tuning vector summarized the center of mass of each neuron's spatial receptive field. Each vector had three components, representing contralateral versus ipsilateral (x), front versus back (y), and up versus down (z) preference.

Spatial selectivity was quantified using two similarly complementary metrics. The first, tuning area, was the fraction of space for which the firing rate was greater than 50% of the maximum firing rate. The second, tuning vector magnitude, was the norm (length) of the tuning vector. Tuning vector magnitude is sensitive to shape and dispersion as well as extent of spatial receptive fields. For example, a hypothetical neuron firing equally strongly to two locations opposite each other in space, and not at all to other locations, would have a small tuning area (~0.1) indicating sharp spatial tuning, but also a tuning vector magnitude of 0, reflecting the lack of directionality.

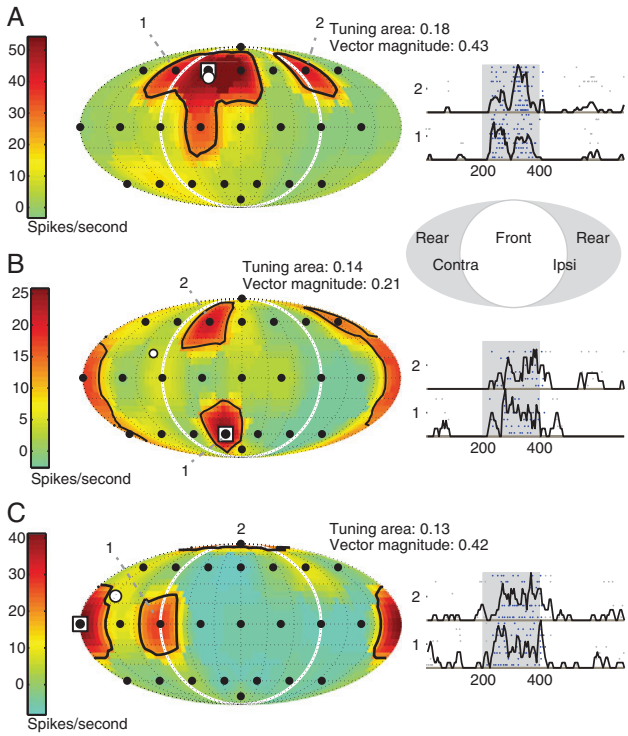

Figure 4. Multi-peaked spatial receptive fields. Receptive fields illustrated as in Figure 3, with interpolated firing rates on the left and peristimulus time histograms and spike rasters on the right. Spatial receptive fields are illustrated using the format described in Figure 3. "Multi-peak" receptive fields contained more than one independent region with interpolated firing rates greater than 50% of the max firing rate. Multi-peaked units were further classified as having well-defined peaks in the lateral dimension (*A*, example unit - noise, 85 dB SPL, A1), along the median plane (*B*, noise, 65 dB SPL, CM/CL), or both (**C**, noise, 65 dB SPL, CM/CL). In these units, local firing rate maxima were separated by local rate minimum, which was less than 50% of the lesser of the first two. For the circular median plane, two local minima were required. Key illustrating layout of the 2D spatial projection, as in Figure 1*B*, is inset.

The spatial receptive field for such a hypothetical neuron would have two "peaks." A large portion of neurons in our sample (173/648, 27%) possessed such fractured, multi-peak spatial receptive fields (Fig. 4), where each contiguous region of the interpolated receptive field in which firing rates were greater than 50% of the maximum firing rate constituted a peak. A majority of multi-peak neurons (120/173, 69% of all multi-peak neurons and 19% of all units) had two peaks. Most multi-peak neurons could be further classified (see Materials and Methods) as being fractured in the lateral dimension (12 units, Fig. 4*A*), the median plane (80 units, Fig. 4*B*), or both (47 units, Fig. 4*C*). A subset of multi-peak neurons (32/173) had relatively minor variations in firing rate near the standard 50% max firing rate threshold; these units were not classified further. Two additional units responded to all locations in the median plane but were not responsive to locations nearest the median plane (front–below and back–above), resulting in two peaks in the interpolated spatial receptive field.

Distribution of Spatial Tuning in Auditory Cortex: Directional Preference

Distributions of best locations and tuning vectors of all sampled neurons are shown in Figure 5*A* for three cortical areas, A1, R/RT, and CM/CL, using the "best" receptive field from each neuron (see Materials and Methods). Note that all neural recordings were made in the left hemisphere (contralateral to the right speaker locations). The majority of neurons responded most strongly to locations in the contralateral hemifield, a trend that was strongest in CM/CL and weakest in R/RT. Within each hemifield, however, there were relatively small variations in the population mean of normalized firing rates (Fig. 5*B*). Tuning vectors tended to be oriented toward the most contralateral locations (Fig. 5*A*), with 36% (148/408), 41% (58/143), and 29% (28/97) of neurons in A1, CM/CL, and R/RT, respectively, having normalized lateral (x) components of −1 to −0.8 (vectors normalized to unit magnitude, with −1 signifying a tuning vector pointing to 90° contralateral). However, the correlation between laterality and firing rates within the contralateral hemifield (including the median plane, for 18 total locations) was weak (A1: $r = 0.039$, $P = 0.0021$; CM/CL: $r = 0.02$, $P = 0.42$; R/RT: $r = -0.013$, $P = 0.61$). This apparent discrepancy can be explained by a portion of neurons with vector averages centered at most contralateral locations while not firing strongly at the most contralateral locations (e.g., a neuron that has a small contralateral bias but has little median plane sensitivity, such as in Fig. 4*B*). There were a substantial number of ipsilateral preferring neurons: by tuning vectors, there were 180 ipsilateral versus 468 contralateral preferring neurons (28%), and using best location (not including median-plane–preferring neurons), there were 119 ipsilateral versus 326 contralateral preferring neurons (27%). Ipsilateral preferring neurons were distributed throughout the hemifield. Data in Figure 5*A*,*B* indicate that spatial receptive fields in A1, CM/CL, and R/RT could cover the entire space surrounding an animal even if a single hemisphere is considered (Fig. 5).

Distribution of Spatial Tuning in Auditory Cortex: Spatial Selectivity

We found a large number of narrowly tuned neurons, particularly in A1 and CM/CL, having spatial receptive fields covering less than 25% of the spatial field (tuning area measure < 0.25, A1:206/408; CM/CL: 103/143; R/RT: 35/97, Fig. 5*C*). Cortical areas R/RT had the largest tuning areas (median = 0.34, interquartile range (IQR) = 0.47), followed by A1 (median = 0.24, IQR = 0.39), and CM/CL (median = 0.14, IQR = 0.21) (Kruskal–Wallis test, $\chi^2(2) = 34.5$, $P = 3.2 \times 10^{-8}$). In contrast, the tendency of neurons to have relatively small tuning vector magnitudes indicates that many neurons displayed spatially dispersed receptive fields (such as Fig. 4*B*) or else were not tuned sharply in both azimuth and elevation (e.g., see Fig. 3*A*). Though narrow tuning area does not guarantee a large tuning vector magnitude, we did find that tuning vector magnitude followed the same trend with regard to cortical area as tuning area (Kruskal–Wallis test, $\chi^2(2) = 73.5$, $P = 1.4 \times 10^{-16}$), with CM/CL having the most directional neurons (median = 0.36, IQR = 0.26), followed by A1 (median = 0.23, IQR = 0.27), and R/RT (median = 0.12, IQR = 0.12).

Due to the range of spatial preferences, we asked whether neurons preferring different regions of space would have different selectivity properties. Qualitatively, Figure 5*A* shows that there were highly selective neurons as defined by tuning vector magnitude that preferred all regions of space. Quantitatively, we compared tuning area, tuning vector magnitude, and number of peaks for contralateral and ipsilateral, lateral and medial, front versus rear, and up- versus down-preferring neurons, as measured by tuning vector direction (see Table 1 for full statistics). Tuning vector magnitudes were significantly larger for contralateral versus ipsilateral preferring neurons, while lateral preferring neurons had larger tuning vectors and fewer peaks, but also larger tuning areas than medial preferring neurons. We also

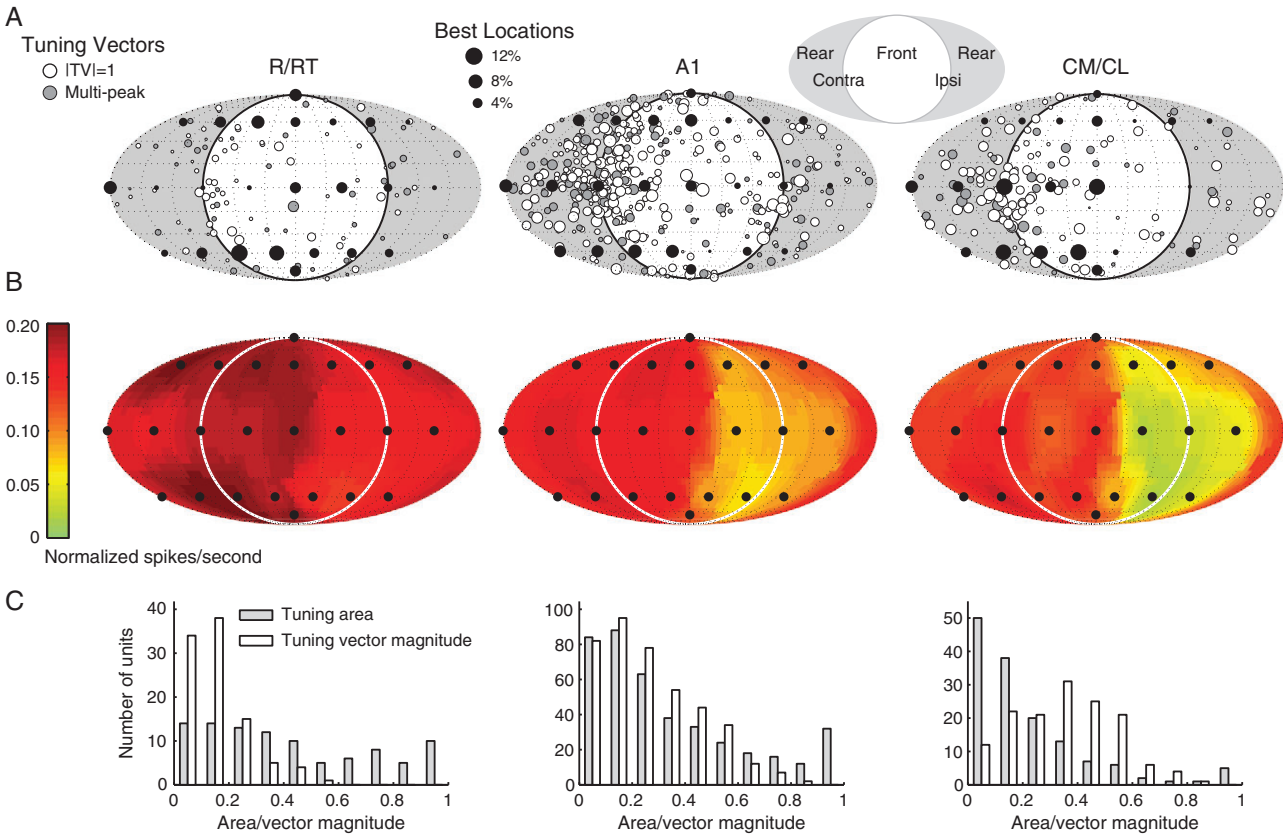

Figure 5. Distribution of spatial tuning in auditory cortex areas A1, CM/CL, and R/RT. (*A*) Histogram of best locations and distributions of tuning vector locations. White and gray circles indicate individual tuning vectors; their magnitudes (|TV|, a larger tuning vector magnitude indicates a more directional receptive field) are indicated by the size of the circles. Gray circles represent neurons with multi-peak receptive fields. The fraction of neurons preferring each individual location is indicated by the size of filled black circles at actual speaker positions (several reference sizes are located top left; see Fig. 1 for a detailed illustration of speaker locations). Key illustrating layout of the 2D spatial projection, as in Figure 1*B* is inset. All auditory areas had tuning vectors and best locations located throughout the full spatial field ($N = 408$ units in A1, 143 in CM/CL, and 97 in R/RT). (*B*) Mean of normalized firing rates across each area. Rates were higher in the contralateral hemifield than the ipsilateral hemifield, but this trend was weaker in A1 and R/RT than in CM/CL. (*C*) Distribution of spatial selectivity in A1, CM/CL, and R/RT. Tuning areas (gray) were highly variable and were largest in R/RT (median = 0.34, interquartile range (IQR) = 0.47), followed by A1 (median = 0.24, IQR = 0.39), and CM/CL (median = 0.14, IQR = 0.21) (Kruskal–Wallis one-way analysis of variance, $P = 2.2 \times 10^{-8}$). Tuning vector magnitude (white) is sensitive to shape and dispersion as well as extent of spatial receptive fields, with higher values associated with less dispersed, more directional receptive fields. CM/CL contained the most directional neurons (median = 0.36, IQR = 0.26; $P = 6.0 \times 10^{-17}$), followed by A1 (median = 0.23, IQR = 0.27), and R/RT (median = 0.12, IQR = 0.12). The receptive field measured with each neuron's preferred stimulus was used for population analyses (see Materials and Methods).

Table 1 Comparison of spatial tuning properties for neurons preferring different regions of space.

	Contralateral preferring $N = 468$	Ipsilateral preferring $N = 180$	Lateral preferring $N = 356$	Medial preferring $N = 292$	Front preferring $N = 307$	Rear preferring $N = 341$	Up preferring $N = 339$	Down preferring $N = 309$
Tuning area	0.22 (0.36)	0.24 (0.41)	0.27 (0.37)	0.18 (0.34)	0.22 (0.36)	0.23 (0.37)	0.28 (0.41)	0.18 (0.31)
	$P = 0.20$		**$P = 1.4 \times 10^{-4}$**		$P = 0.98$		**$P = 1.1 \times 10^{-5}$**	
Vector magnitude	0.25 (0.30)	0.18 (0.25)	0.26 (0.29)	0.20 (0.26)	0.23 (0.27)	0.24 (0.29)	0.21 (0.25)	0.26 (0.31)
	$P = 2.4 \times 10^{-5}$		**$P = 2.7 \times 10^{-4}$**		$P = 0.76$		**$P = 0.0012$**	
Number of peaks	1.3 ± 0.7	1.4 ± 0.8	1.3 ± 0.7	1.4 ± 0.8	1.3 ± 0.8	1.3 ± 0.7	1.3	1.3
	$P = 0.17$		$P = 0.065$		$P = 0.49$		$P = 0.94$	

Median and interquartile range (in parentheses) are given for tuning area and tuning vector magnitude, while mean and standard deviation are given for number of peaks. Directional preference classifications were determined based on tuning vectors. A neuron was considered lateral preferring if its tuning vector was within 45 degrees of either of the most lateral speaker locations. Wilcoxon rank-sum test results are listed beneath summary statistics. Bold font represents statistically significant *P*-values.

found that down-preferring neurons were substantially more selective, with smaller tuning areas and larger tuning vector magnitudes. For the comparison between front- and rear-preferring neurons, all three measures were similar.

Dependence of Spatial Tuning Selectivity on Best Frequency

The availability and neural processing of spatial cues is frequency dependent. Interaural time differences are the dominant

spatial cue at low frequencies, whereas interaural level differences and monaural spectral shape features are perceptually dominant at higher frequencies (Blauert 1997). In marmosets, interaural level differences increase from approximately 1 kHz to 12 kHz, whereas the most reliable monaural spectral cues (i.e., the first spectral notch) are between 12 and 24 kHz (Slee and Young 2010). Because of the fact that our stimuli contained energy outside the frequency range that interaural time differences are thought to dominate sound localization (Blauert 1997), it is possible that neurons receiving high-frequency information received stronger binaural and spectral information for sound localization in the present experiment.

The distribution of BF (Fig. 2) was different in A1 (median = 11.4 kHz, IQR = 12.2 kHz for 171 units tested for BF and spatial tuning), CM/CL (median = 16 kHz, IQR = 19.7 kHz, $n = 45$), and R/RT (median = 4 kHz, IQR = 4.4 kHz, $n = 50$; Kruskal–Wallis test, $\chi^2(2) = 22.2$, $P = 1.5 \times 10^{-5}$). Pooling all units, there was a weak negative correlation between BF and tuning area ($r = -0.23$, $P = 1.4 \times 10^{-4}$, $n = 266$) and a weak positive correlation between BF and tuning vector magnitude ($r = 0.22$, $P = 2.86 \times 10^{-4}$). In individual areas, correlations reached statistical significance for A1 (tuning area: $r = -0.25$, $P = 9.61 \times 10^{-4}$; tuning vector magnitude: $r = 0.2$, $P = 0.01$). R/RT had a similar effect size for tuning area ($r = -0.25$, $P = 0.079$), but not for tuning vector magnitude ($r = -0.003$, $P = 0.98$). In our CM/CL samples, BF and tuning selectivity were not correlated (tuning area: $r = -0.05$, $P = 0.74$; tuning vector magnitude: $r = 0.06$, $P = 0.7$). To determine the extent to which the combination of BF bias and BF spatial selectivity correlations contributed to the apparent spatial selectivity differences between cortical areas, we first performed an analysis of covariance of BF and tuning area/tuning vector magnitude. There was a main effect of cortical area on tuning area between A1 and CM/CL ($F = 6.83$, $P = 0.0096$) but not tuning vector magnitude ($F = 2.19$, $P = 0.14$), and a main effect on tuning vector magnitude between A1 and RT ($F = 8.82$, $P = 0.033$) but not tuning area ($F = 0.12$, $P = 0.73$). Between CM/CL and R/RT, there were main effects of tuning area ($F = 5.17$, $P = 0.025$) and tuning vector magnitude ($F = 19.38$, $P = 2.9 \times 10^{-4}$). These results are consistent with BF spatial selectivity correlations. Second, we performed simple statistical tests between neurons from R/RT and CM/CL each with those from A1, but only including the spatial fraction of A1 along the BF axis (extending from the low BF and high BF borders, respectively) for which the median BF-matched each area. This analysis included all neurons within the determined areas, regardless of whether BF was obtained. When comparing "CM/CL BF-matched" A1 and CM/CL ($n = 152$, 143), results were consistent with the analysis of the complete dataset, while effects were smaller. Tuning area was higher in A1 (median = 0.21 vs 0.14, $P = 0.048$, Wilcoxon rank-sum test), and tuning vector magnitude was lower (median = 0.30 vs 0.36, $P = 0.018$). For "R/RT BF-matched" A1 and R/RT ($n = 59$, 97), the results of the comparisons were not consistent with the complete sample. Tuning area (median = 0.43 for A1 vs 0.35 for R/RT, $P = 0.64$) and tuning vector magnitude (median = 0.13 for A1 vs 0.12 for R/RT, $P = 0.11$) were not significantly different. We did not attempt to obtain BF-matched samples between CM/CL and R/RT, though the sample sizes would have been small.

These tests indicate that BF and tuning selectivity interact and that the strength of the inference that tuning selectivity increases along the rostral to caudal axis may hinge on this dependence, in particular for R/RT. However, previous studies have consistently reported biases in cochleotopic representation qualitatively similar to those found in the present dataset (Merzenich and Brugge 1973; Morel et al. 1993; Kosaki et al. 1997; Rauschecker et al. 1997; Recanzone et al. 2000; Bendor and Wang 2008; Zhou and Wang 2012). We therefore have not controlled for BF in the remainder of the analyses.

Effects of Sound Level on Spatial Tuning Properties

Studies of spatial tuning in anesthetized animals have found that spatial receptive fields generally increase in size with increasing sound level (Middlebrooks and Pettigrew 1981; Brugge et al. 1996; Stecker et al. 2003; Mrsic-Flogel et al. 2005). Such a sound level dependency has been found to be weaker or non-significant in azimuth and partial space tuning in awake animals (Eisenman 1974; Mickey and Middlebrooks 2003; Woods et al. 2006; Zhou and Wang 2012). In the present study, it was common to find neurons with spatial tuning which was qualitatively similar across sound level. Two such units are shown in Figure 6. At the population level (Fig. 7A–C), we found a weak positive correlation between sound level and tuning area in A1 (716 total measurements in 408 units, $r = 0.15$, $P = 6.6 \times 10^{-5}$) and R/RT (221 measurements in 97 units, $r = 0.13$, $P = 0.046$), but not in CM/CL (239 measurements in 143 units, $r = -0.032$, $P = 0.63$). Note that the effect in R/RT is not significant at the Bonferroni-corrected alpha level of 0.017, though identifying an effect of such a magnitude would not be possible with the present sample size, in contrast with A1. Effects of sound level on tuning vector magnitude were similar: there was a small but significant effect of sound level on tuning vector magnitude in area A1 ($r = -0.14$, $P = 1 \times 10^{-4}$), but there was no effect in CM/CL ($r = -0.006$, $P = 0.9$) or R/RT ($r = -0.011$, $P = 0.87$). For the subset of neurons in which spatial tuning was measured at multiple sound levels (median number of sound levels tested equal to 2 for those tested at multiple levels) and/or multiple times at a single level ($n = 212/163$/total 291 units), the effects of sound level on single-neuron tuning properties were quantified by comparing the additional receptive field measurements to the "best" spatial receptive field (selected as having the highest single firing rate across all stimulus sets tested—see Materials and Methods). First, we computed the correlation between the change in tuning area and the change of sound level (Fig. 7D–F; ΔdB SPL, referenced to level of the best spatial receptive field). There were no significant correlations between change in tuning area and ΔdB SPL in A1 (336 additional measurements in 130/90/176 units, $r = 0.093$, $P = 0.088$) or R/T (124 additional measurements in 41/39/57 units, $r = -0.01$, $P = 0.3$), but there was a significant negative correlation between tuning area and ΔdB SPL in CM/CL (97 additional measurements in 41/32/58 units, $r = -0.32$, $P = 0.0013$), indicating that spatial selectivity actually increased with sound level in this area. This analysis was repeated using tuning vector magnitude instead of tuning area, and no correlation was found in any cortical area between tuning vector magnitude and ΔdB SPL. In general, changes in tuning area and vector magnitude within single neurons were small, typically 0.1 or less across all areas and ΔdB SPL values and were of similar magnitude to changes measured when retesting at the same sound level (ΔdB SPL = 0). Finally, we measured the change in tuning vector direction (angle, in degrees) as a function of ΔdB SPL (Fig. 7G–I) finding weak effects in A1 ($r = 0.19$, $P = 0.00039$) and R/RT ($r = 0.26$, $P = 0.0033$), but not CM/CL ($r = 0.098$, $P = 0.33$). Thus, the present results are in agreement with other recent results in awake animals suggesting minimal effects of sound level on spatial tuning in auditory cortex.

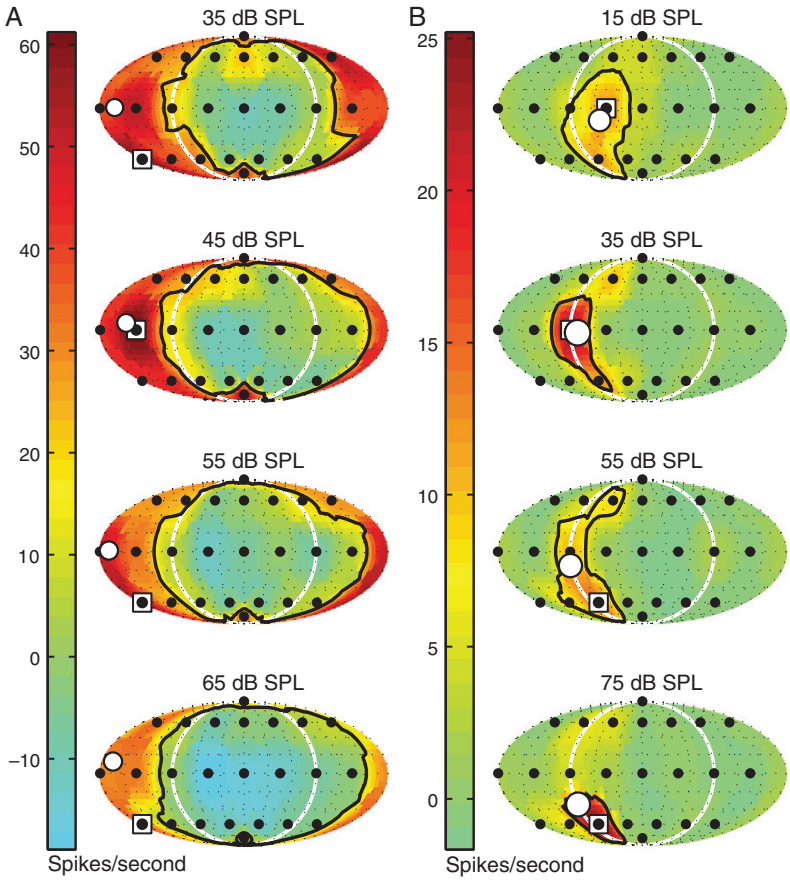

Figure 6. Examples of receptive fields measured at multiple sound levels. (*A*) Rear-preferring neuron (noise, A1) shows tuning-preferred direction and tuning area is preserved across sound level. (*B*) Contralateral preferring neuron (noise, CM/CL). Spatial receptive fields are illustrated using the format described in Figure 3.

Euclidean Distance Between Population Responses Associated with Different Sound Locations

Previous studies based on spatial tuning in azimuth (Tian et al. 2001; Stecker et al. 2003; Woods et al. 2006) and elevation (Stecker et al. 2003) have suggested that caudal auditory cortical areas are important for sound localization. We hypothesized that if CM/CL is important for full-field sound localization, population firing rates associated with different locations should be less similar, potentially leading to better neural discrimination. Treating the mean normalized firing rates of the population of neurons associated with each speaker location as a vector, we calculated the Euclidean distance between population firing rates (vectors) for all pairs of locations, normalized by neural population size. Only data from animals with all three areas recorded were included in this analysis (2 animals; A1:245 units; CM/CL: 147 units; R/RT: 97 units). Figure 8*A* shows the resulting Euclidean distance distribution for each area, averaged from the distances between each location and its four "nearest" locations (as measured by population response vectors rather than physical space, see Materials and Methods). Median Euclidean distances over different regions of space are summarized in Figure 8*B*. The averaged Euclidean distance was greater in the contralateral hemifield than the ipsilateral hemifield for A1 (median = 0.30, IQR = 0.02 vs 0.22, IQR = 0.02; Wilcoxon sign-rank test, four nearest distances for nine locations $P = 1.6 \times 10^{-7}$) and CM/CL (median = 0.32, IQR = 0.05 vs 0.19, IQR = 0.06, $P = 1.7 \times 10^{-7}$), suggesting that neighboring locations in the contralateral hemifield are better discriminated by firing rates of the neuronal population. This difference was smaller, but still significant, for R/RT (median = 0.26, IQR = 0.01 vs 0.25, IQR = 0.02, $P = 0.003$) (Fig. 8*A*, left).

Comparing areas, Euclidean distance between the nearest locations was slightly larger in the contralateral hemifield and smaller in the ipsilateral hemifield from R/RT to A1 ($P = 1.1 \times 10^{-6}$ for contralateral, $P = 6.6 \times 10^{-5}$ for ipsilateral) and from A1 to CM/CL ($P = 8.0 \times 10^{-5}$, 6.4×10^{-7}). In the median plane, Euclidean distance was larger in A1 (median = 0.31, IQR = 0.02) and CM/CL (median = 0.31, IQR = 0.04) than in R/RT (median = 0.27, IQR = 0.03; Wilcoxon sign-rank test, four nearest distances for six locations $P = 3.9 \times 10^{-5}$, 5.6×10^{-5}), but there was no significant difference between A1 and CM/CL ($P = 0.95$). Thus, while population responses for pairs of sound source locations in the contralateral hemifield became less similar moving rostrally to caudally in auditory cortex, this was concomitant with an increase in similarity for pairs of ipsilateral locations. This result is consistent with previous studies showing both increased information about contralateral space and stronger spatial selectivity in caudal areas (Tian et al. 2001; Stecker et al. 2003; Woods et al. 2006).

We also used Euclidean distance to compare population selectivity across different regions of space in the front versus rear and vertical axes. We focused on contralateral locations, as the majority of recorded neurons preferred the contralateral hemifield. Consistent with the lack of differences in tuning

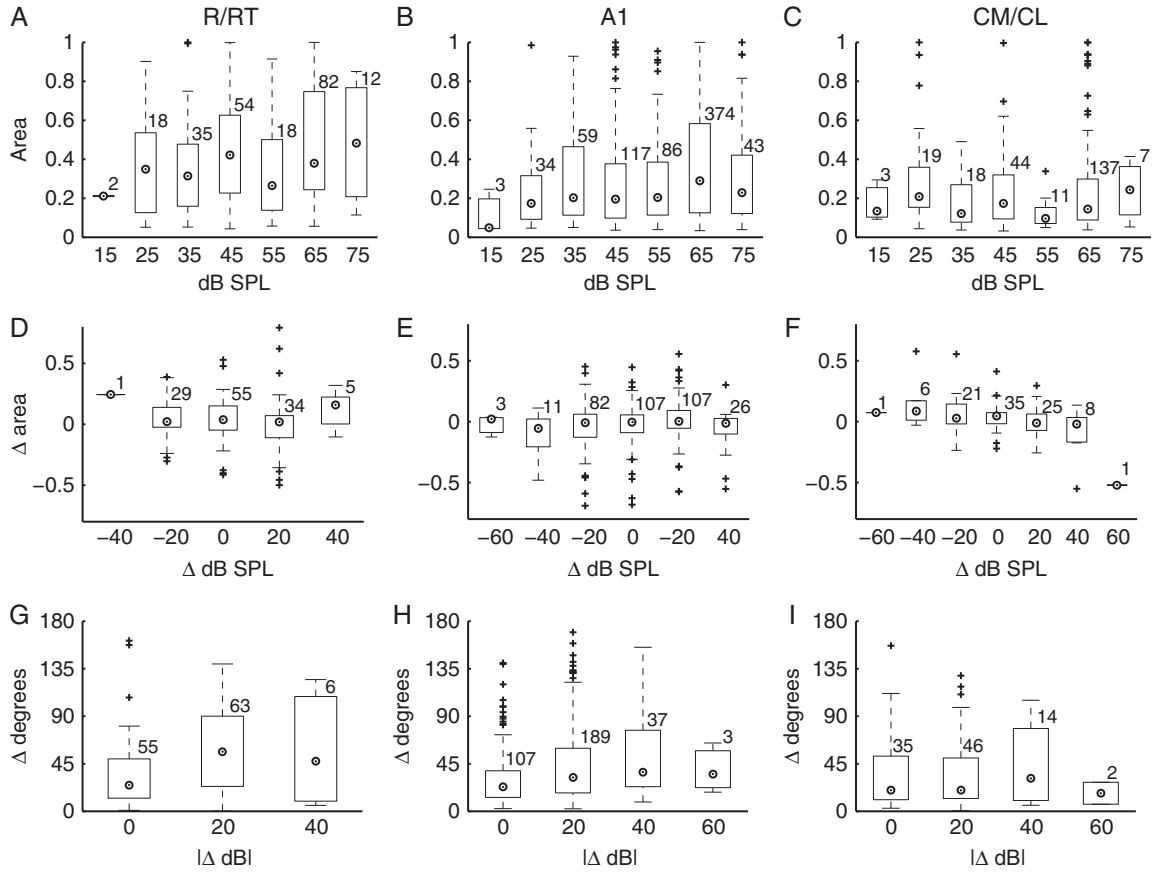

Figure 7. Tuning stability across sound pressure level (dB SPL). (*A–C*) Tuning area versus level. There were weak correlations between sound level and tuning area in A1 ($r = 0.15$, $P = 6.6 \times 10^{-5}$) and R/RT ($r = 0.13$, $P = 0.046$), but not in CM/CL ($r = -0.032$, $P = 0.63$). For tuning vector magnitude, results were similar with weak relationships in A1 ($r = -0.14$, $P = 1 \times 10^{-4}$), CM/CL ($r = -0.006$, $P = 0.9$), and R/RT ($r = -0.011$, $P = 0$ .87). (*D–F*) Within-neuron analysis of level effects on tuning area. Analysis of effects of sound level on spatial selectivity within individual neurons was similar and non-significant for A1 and R/RT, while there was a significant negative correlation between tuning area and sound level in CM/CL units ($r = -0.32$, $P = 0.0013$). (*G–H*) Tuning vector stability versus sound pressure level. Change in tuning vector direction (in degrees) as a function of ΔdB SPL. There were effects of ΔdB SPL on tuning vector shift magnitude in A1 ($r = 0.19$, $P = 0.00039$, Spearman's r) and R/RT ($r = 0.26$, $P = 0.0033$), but not CM/CL ($r = 0.098$, $P = 0.33$). Data points at ΔdB SPL = 0 represent instances when the same level was tested multiple times in the same neuron. All plots were generated using Matlab's boxplot function. For each value on the abscissa, the central mark indicates the median, the edges of the box indicate the 25th and 75th percentiles, and the crosses represent outliers. The number of neurons measured at each sound level is indicated next to each box.

selectivity for neurons preferring front versus rear locations (Table 1), Euclidean distances were not different between front and rear locations for any cortical area. Along the vertical axis, we performed comparisons between locations above, at, and below 0° elevation. Consistent with tendency for neurons preferring the lower hemifield to exhibit higher spatial selectivity, there was a tendency for Euclidean distances to increase from higher to lower elevations (Fig. 8*B*). In CM/CL, nearest Euclidean distances for elevations above 0° (median = 0.29, IQR = 0.01) were significantly smaller than those at 0° (median = 0.33, IQR = 0.03; $P = 1.1 \times 10^{-5}$, Wilcoxon rank-sum test) and below 0° (median = 0.34, IQR = 0.04; $P = 7.3 \times 10^{-7}$). In R/RT, nearest Euclidean distances for elevations above 0° (median = 0.26, IQR = 0.01) were significantly smaller than those below 0° (median = 0.28, IQR = 0.04; $P = 0.009$). Differences were smaller and not significant in A1 (Fig. 8*B*).

Principal Component Analysis of Spatial Receptive Fields

The distribution of tuning vectors (Fig. 5*A*) indicates that spatial receptive fields are broadly distributed across the space around an animal, but the tuning vector does not describe spatial receptive field shape. In order to understand whether receptive field shape, in addition to preferred location and tuning vector direction, carries biologically important information, we performed a principal component analysis to characterize the dimensions along which spatial receptive fields varied most strongly. Like the Euclidean distance analysis above, only data from animals with all three areas recorded were included in the analysis. Here in particular, including data from the subject with only A1 recorded would lead to the A1 units dominating the grouped analysis. The first five resulting principal components are plotted in Figure 9 and can be approximately interpreted in terms of intuitive, biologically relevant spatial dimensions, although none contain information from a single dimension exclusively. The first principal component, accounting for 40% of total variance, approximates the non-directional component of neural responses and is referred to as the spatial response contrast as it is highly correlated with tuning area ($r = 0.96$, $P = 4.9 \times 10^{-257}$). The second and third components reflect neurons' hemifield (contralateral vs ipsilateral) and laterality (central vs lateral) preferences, respectively. These two components together describe variation along azimuth. The fourth

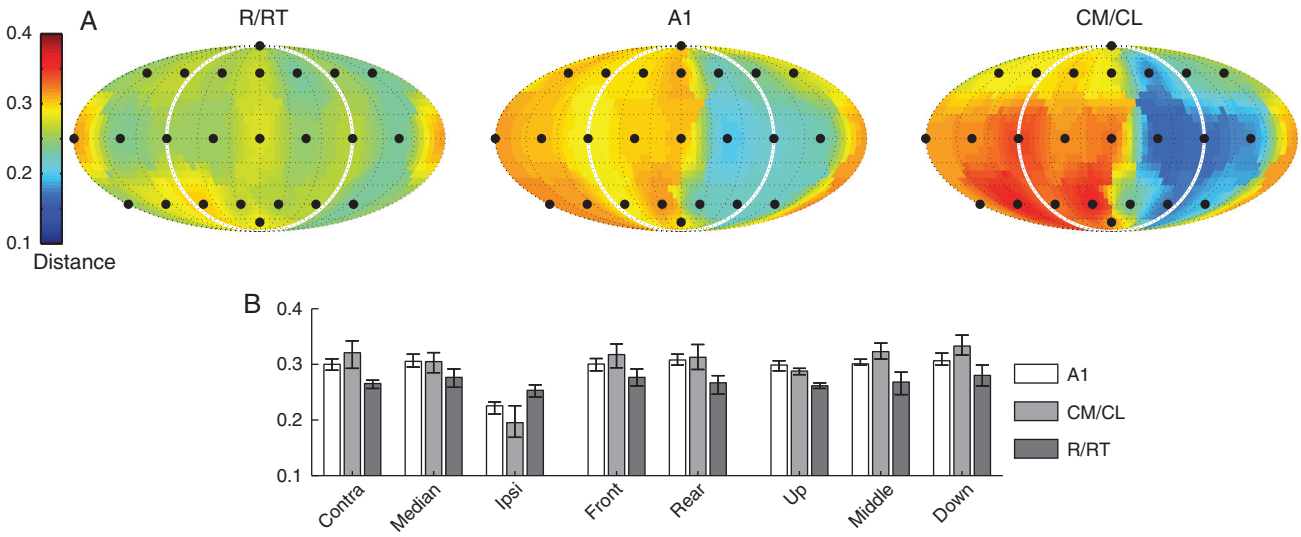

Figure 8. Euclidean distance analysis. (*A*) Euclidean distance between mean scaled population firing rates to pairs of locations, normalized by population size, to the nearest four locations by rate (interpolated for visualization). For all locations, distance between responses was larger in the contralateral hemifield than the ipsilateral hemifield, but this effect was area dependent. From R/RT to A1 to CM/CL, Euclidean distance increased in the contralateral hemifield in and decreased in the ipsilateral hemifield. In the median plane, A1 and CM/CL were similar but were both larger than R/RT. (*B*) Median value of nearest four locations for different regions of space for each area. For front versus back and vertical comparisons, only medial and contralateral locations are included. Error bars indicate IQR. See text for numeric comparisons.

and fifth components represent front/back and up/down variation, respectively. Variation in azimuth makes up a larger fraction of variance than variation in the median plane (18% vs 10%), while the remaining components (6–24) were less intuitive and constituted the final 32% of variance.

Analysis of Spatial Receptive Field Shape Clustering and Topographic Organization

Although we have provided examples of "classes" of spatial receptive fields (e.g., contralateral, ipsilateral, front, and rear preferring), the distribution of tuning parameters (Fig. 5A,C) suggest a continuous distribution. Likewise, previous work has shown that binaural sensitivity varies continuously throughout auditory cortex despite the frequent use of classification schemes in the literature (Campbell et al. 2006). It is possible, however, that clusters of receptive field classes could exist yet be indiscernible without considering full-field spatial receptive fields. We therefore applied *k*-means clustering on both the first five principal components and the full 24 principal components and used the gap statistic method (Tibshirani et al. 2001) to analyze the results. Strong evidence for clusters was not found; the largest increase in the gap value was smaller than the value for one cluster. The cluster centers for $k = 2$, primarily separated by the strength of non-directional response (component 1) are shown in Figure 10A. Though there were no clear clusters in receptive field shape across the entire population, it was still a possibility that spatial receptive fields could be quantitatively different across areas. We trained a series of linear support vector machine classifiers in "one versus rest" configurations to classify populations from each area against the remaining two. Classification performance was generally poor using full spatial receptive fields (accuracy: 0.50 for A1; 0.64 for CM/CL; 0.61 for R/RT) and principal components 1–5 (accuracy: 0.50 for A1; 0.66 for CM/CL; 0.58 for R/RT). These results show that there is substantial overlap in spatial receptive field shape between areas in auditory cortex.

Another common observation in studies of spatial representation in auditory cortex is the lack of a topographical "map" of auditory space (Middlebrooks 2014). However, this question has not been addressed for full-field spatial tuning in awake mammals. Figure 10B–D illustrates the topographic distribution of normalized tuning vector components. No map of auditory space was apparent, for contralateral versus ipsilateral, front versus back, or up versus down selectivity. We further tested for the possibility that, even in the absence of a spatial map, neurons recorded within single or nearby recording tracks might still share similar directional preferences. To do this, we calculated the correlation coefficient between 1) the angles between the tuning vectors of all pairs of neurons and 2) the physical distances between the recording tracks in which neurons were recorded (distance = 0 for neurons recorded in the same track). This correlation was small and not significant in A1 ($r = 0.015$, $P = 0.15$; permutation test, $n = 1000$ permutations), CM/CL ($r = -0.03$, $P = 0.43$), and R/RT ($r = 0.03$, $P = 0.23$), indicating a lack of evidence for clustering or topographical organization in general.

Discussion

By measuring responses to a full-field speaker array, we found that the entire auditory space around a marmoset was represented across neuronal populations in cortical fields A1, CM/CL, and R/RT. This sampling of space provided a more complete description of spatial tuning; in many cases, commonly used subsampling techniques would have missed important response features or failed to drive neurons entirely. Distributions of best locations and tuning vectors, as well as principal component analysis of receptive fields, revealed that variations in spatial tuning occurred along biologically relevant dimensions, with the first five principal components representing roughly response contrast (selectivity), hemifield preference, laterality, up/down variability, and front/back variability. Of the directional principal components (#2-5), hemifield preference accounted for the most

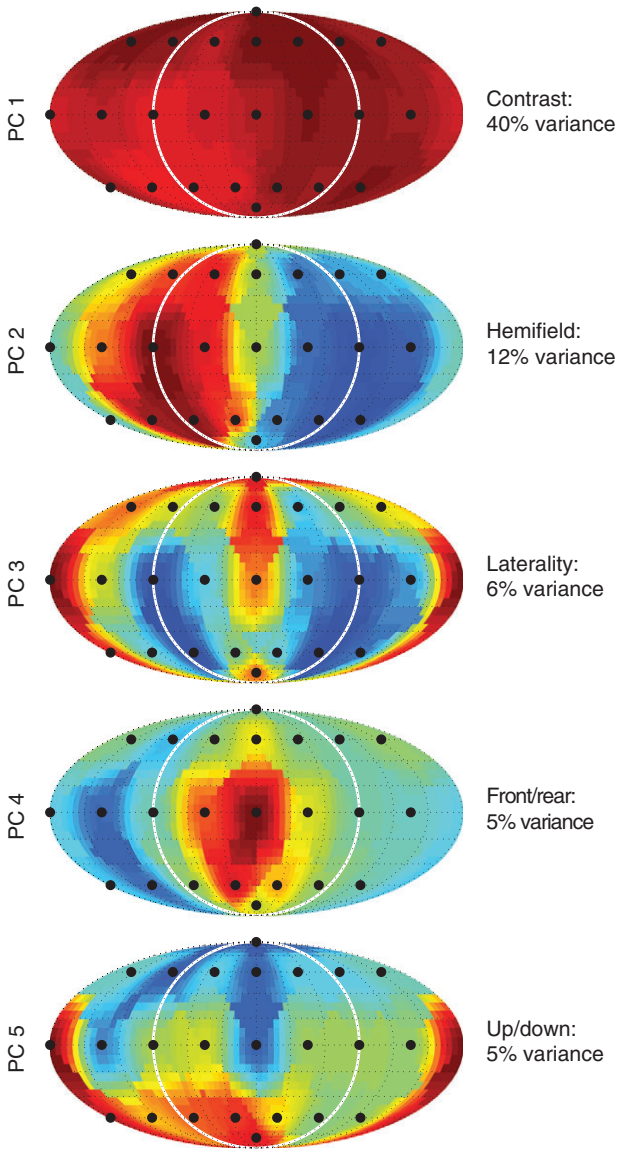

Figure 9. Principal component analysis. Principal component analysis was performed on normalized spatial receptive fields across cortical areas. The individual principal components (PCs) can be approximately interpreted in terms of biologically relevant spatial dimensions. The first principal component (40% of receptive field variance) is not highly directional and is referred to as "contrast." The second and third components (12% and 6% of variance) reflect neurons' hemifield and laterality preference and together describe azimuth tuning. The fourth and fifth components represent front/back (5% of variance) and up/down variation (5% of variance).

variability across the population. Despite a contralateral bias of spatial receptive fields that increased from R/RT to A1 to CM/CL, a substantial number of neurons were tuned to the ipsilateral hemifield in all cortical areas. We did not find strong evidence for clusters of receptive field shapes or a topographical map of auditory space, in agreement with previous work suggesting a continuous (Campbell et al. 2006), spatially heterogenous (Middlebrooks 2014) distribution of spatial preference in auditory cortex, although we note that the present experiment does not rule out the possibility for topographic clustering on a finer spatial scale (≥100 μm between tracks) than was achieved in the current experiment.

The majority of neurons, particularly in areas A1 and CM/CL, had relatively small tuning areas, with responses greater than half the maximum firing rate frequently encompassing less than 25% of space. A complementary measure of directionality, the tuning vector magnitude, which is sensitive to dispersion of spatial receptive fields, showed that for many neurons, directionality was not very high. This was due to the fact that neurons could have non-contiguous receptive fields, or be narrowly tuned in only a single dimension. Tuning area, vector, and vector magnitude measured in auditory cortex of awake marmosets were found to be relatively insensitive to changes in sound level.

Comparing neurons that preferred contralateral versus ipsilateral or lateral versus medial regions of space, we found that lateral preferring neurons and contralateral preferring neurons in particular had the highest spatial selectivity. This was not the rule, however, as we found highly directional neurons tuned to all regions of space (e.g., Fig. 3*B–D* and Fig. 5*A* for summary). While the finding that medial preferring neurons were more selective by the area measure was unexpected, the tendency for medial preferring neurons to have more dispersed spatial tuning is perhaps not surprising. Although spatial localization in the median plane can be accurate, listeners can make large errors such as confusing front versus back locations (Makous and Middlebrooks 1990).

We also compared tuning selectivity for front and rear locations and along the vertical axis. We did not find any difference in the tuning properties of front versus rear-preferring neurons, and population selectivity as measured by Euclidean distances of population firing rates was consistent with this observation. However, there was a substantial difference in selectivity along the vertical axis, with higher generally lower selectivity above 0° elevation. A possible explanation for this observation is acoustics: in marmosets, the most extreme values of both ILD and ITD can be found below 0° elevation (Slee and Young 2010).

Comparison with Previous Studies

Studies of full-field spatial tuning in anesthetized animals have observed receptive fields that are typically centered in the contralateral–frontal quadrant of space, along the "acoustic axis" of the ear (Middlebrooks and Pettigrew 1981; Brugge et al. 1994, 1996; Schnupp et al. 2001; Mrsic-Flogel et al. 2005). These studies suggested that spatial tuning is far less diverse than that found here. They also reported that as sound levels increase, receptive fields broadened, often substantially. This pattern of neural responses has been observed in partial field studies of anesthetized animals as well (Middlebrooks et al. 1994; Middlebrooks and Xu 1998; Stecker et al. 2003). Recent studies of partial field tuning in awake animals have found more modest degradation in spatial tuning selectivity with increasing sound level, as well as more evenly distributed location preferences (Mickey and Middlebrooks 2003; Woods et al. 2006; Zhou and Wang 2012; Lee and Middlebrooks 2013). It has been suggested that even in awake macaques, neurons largely prefer the contralateral pole (Werner-Reiss and Groh 2008), although this conclusion was based on fitted tuning functions that do not capture all of the information in the underlying spatial receptive fields. In agreement with and extending the majority of recent work, we showed that there is a broad distribution of spatial receptive fields across the entire spatial field. We also found that both tuning area and tuning vector magnitude were stable across sound levels within single neurons, providing

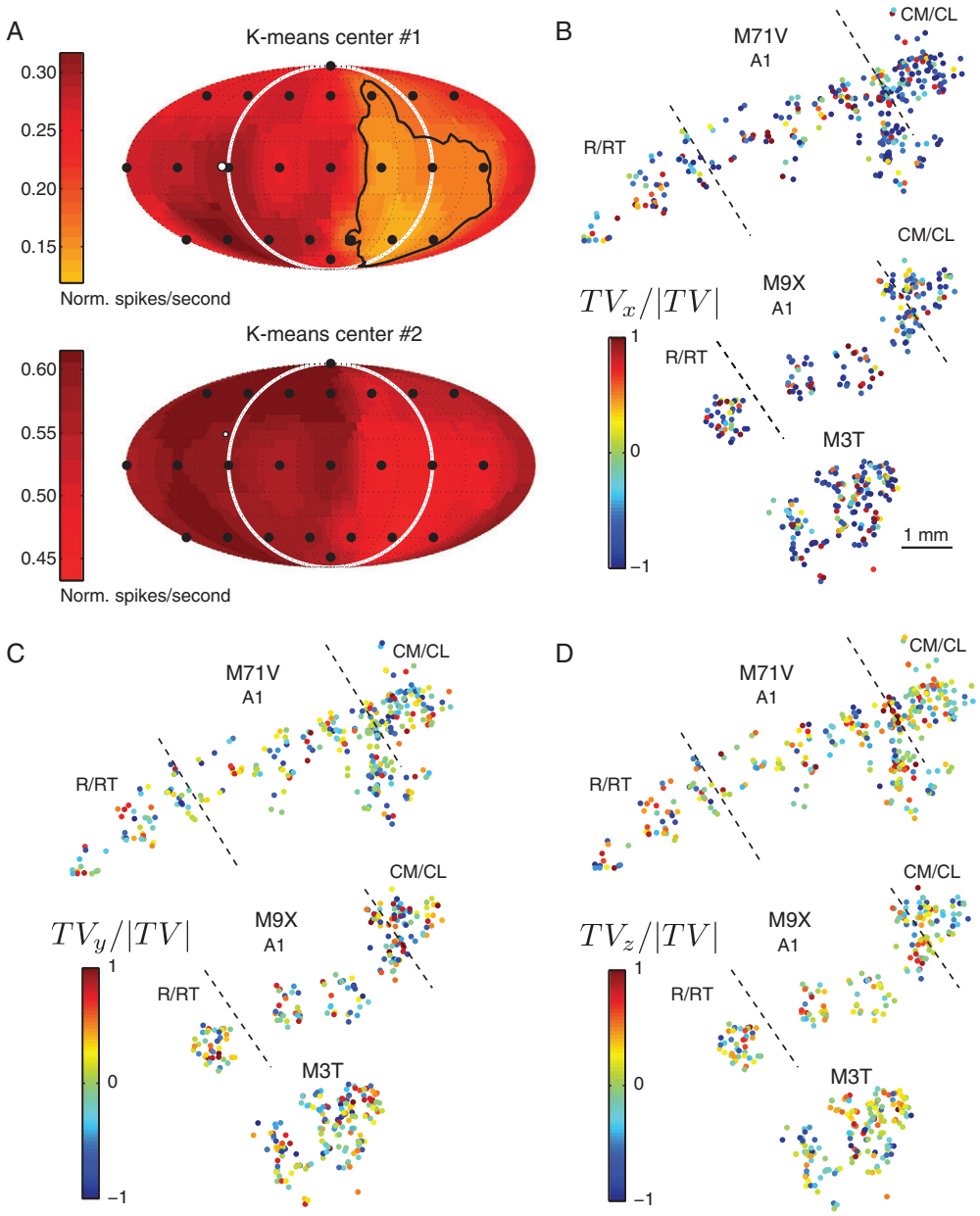

Figure 10. Clustering results and topographic distributions of directional preference. (A) Spatial receptive field *k*-means cluster centers. We tested the 24D normalized spatial receptive fields for evidence of clustering using *k*-means clustering and the gap statistic (see Materials and Methods). Evidence for clustering was not found. The cluster centers for $k = 2$, shown above, were primarily separated by the strength of non-directional response (i.e., PCA component 1, see Fig. 9). (*B–D*) Topographic distribution of lateral (*x*, *B*), front versus back (*y*, *C*), and up versus down (*z*, *D*) directional preferences. Format like Figure 2. Colored circles represent the value of individual tuning vector components normalized by the tuning vector magnitude for each neuron. No topographic organization of directional preference was apparent in any of the areas recorded. As in Figure 2, the position of recorded units was jittered slightly in order to visualize multiple units in each recording track.

evidence that the stability of spatial tuning in awake animals across sound level extends to the full spatial field.

The mechanisms underlying the differences in spatial tuning between anesthetized and awake conditions are not known. However, receptive fields in A1 of anesthetized animals have been shown through the use of closed-field sound delivery to be largely explained by a linear superposition of frequency and binaural cues (Schnupp et al. 2001), while studies of spectral processing in awake animals have shown that nonlinear interactions play a role in shaping responses in awake animals (Barbour and Wang 2003; Kadia and Wang 2003; Sadagopan and Wang 2008). Various anesthetics have been observed to both reduce (Zurita et al. 1994; Gaese and Ostwald 2001) and increase (Guo et al. 2012) frequency tuning selectivity under anesthesia, even as preferred frequency has been shown to be largely preserved. Thus, changes in spectral integration under anesthesia may degrade full-field spatial representations, which rely on integrating information across frequency (Blauert 1997). Future closed-field studies in awake animals are necessary to measure linear and nonlinear interactions between binaural and spectral cues. This technique has been used to study auditory cortex in anesthetized animals (Brugge et al. 1994, 1996; Schnupp et al. 2001; Mrsic-Flogel et al. 2005), and it has been recently used in awake

marmosets to study binaural processing in the inferior colliculus (Slee and Young 2011, 2013).

It is possible that there exist species-specific differences in spatial tuning properties in auditory cortex. Receptive fields in awake cats typically span an entire hemifield, with many neurons responding omnidirectionally (Mickey and Middlebrooks 2003; Lee and Middlebrooks 2011, 2013). In one study, median tuning areas as high as 294° were measured in primary auditory cortex (Lee and Middlebrooks 2011), which is equivalent to tuning area of about 0.8. In a full-field study in anesthetized ferrets, spatial receptive fields rarely exceeded a hemifield in size (Mrsic-Flogel et al. 2005). In a study of awake macaques, tuning was sharper still, with median tuning areas ranging from ~90° to ~270° in A1 (0.25–0.75) to ~90° (0.25) in CL (Woods et al. 2006). Differences exist in tuning preferences in addition to selectivity: a recent study in anesthetized rats found that neurons in auditory cortex were exclusively tuned to the contralateral hemifield, an observation that to our knowledge has not been made in other species (Yao et al. 2013). Thus, it is possible that spatial coding strategies may vary among mammalian species.

A limitation of the current study is the relatively coarse speaker spacing. While we speculate that the present results would not change qualitatively, details could be refined by sampling more densely in space. For example, the lower bound on tuning area is directly related to speaker spacing, and it is likely that the present study overestimated tuning area for many neurons. It is also possible that some of the multi-peaked neurons actually have fully contiguous receptive fields, which would only be revealed by a denser sampling (such as that shown in Fig. 4*B*, for instance). A denser speaker spacing would also allow direct comparison of azimuth tuning selectivity between marmoset and other species, which would be important to address in future studies.

Potential Dependence of Spatial Tuning on Behavioral Context

A full understanding of spatial processing in auditory cortex must account for any dependence of spatial representation on behavioral context. The available evidence from auditory cortex of in awake and behaving animals indicates that such dependence is largely modulatory, comprising changes in gain or sharpness of tuning. In an early study (Benson et al. 1981), macaque monkeys were trained to either localize or detect a sound coming from one of five locations. Neural responses in both conditions were most commonly not significantly different during behavior compared with passive listening, although a substantial minority displayed increased firing rates, and a small minority displayed decreased firing rates. Response differences across the detection and localization tasks were less frequent, and changes in the preferred location in single neurons were not reported. Comparable results were reported in a later study in which macaques detected changes in interaural phase differences (Scott et al. 2007). While firing rates commonly increased during task performance relative to passive listening, no shifts in interaural phase difference tuning were found. This is perhaps not all that surprising because animals should be able to localize sounds even if not a priori engaged in a localization task, which argues for the importance of spatial tuning by auditory neurons in the "resting state" (i.e., non-behaving condition).

A pair of studies by Lee and Middlebrooks (2011, 2013) measured spatial tuning through 360 degrees azimuth in the behaving condition relative to passive. Here, the authors compared spatial tuning across multiple behavioral contexts (passive listening and periodicity detection and localization tasks) in several cortical areas in cats and found that the primary effect of engagement in both tasks on spatial tuning was a sharpening of tuning functions (Lee and Middlebrooks 2011, 2013). As in previous studies, no tuning shift was observed, and like the Benson et al. (1981) study, a primary finding was that spatial tuning was largely similar when comparing behavioral tasks, which did or did not require spatial localization. While these studies did not measure the effect of behavior on full-field spatial responses, Lee and Middlebrooks (2011, 2013) did include both front and rear azimuth locations, so any qualitative effects of behavior on spectral cue-dependent spatial representation would have been captured. If behavioral engagement produces a similar effect in marmosets as observed in cats, this would primarily serve to strengthen our finding that many neurons in auditory cortex are highly selective to spatial location.

Despite these findings suggesting that spatial tuning in non-behaving animals is representative of spatial tuning during localization, it is possible that a task in which subjects attend to specific locations in space would result in more substantial changes in tuning preferences in some auditory cortex neurons, analogous to those found for frequency tuning (Fritz et al. 2003). However, as Fritz et al. (2003) showed, the frequency tuning (CF or BF) of A1 neurons remained mostly unchanged even if when an animal engaged in behavioral tasks. Future studies should investigate the neural mechanisms of selective auditory spatial attention.

Spatial Tuning in Primary, Rostral Core, and Caudal Belt Areas

The finding that spatial tuning sharpened along the rostral to caudal dimension is consistent with previous studies in several species, both in anesthetized and awake animals (Recanzone et al. 2000; Tian et al. 2001; Stecker et al. 2003; Woods et al. 2006). We also found that spatial receptive fields are more contralaterally biased in CM/CL, although normalized population firing rates were roughly flat within the contralateral hemifield in all areas. This increase in firing rates to contralateral locations also translated to an increase in population firing rate separation between different locations, measured by Euclidean distance, in the contralateral hemifield. However, this increase came at the expense of population distance in the ipsilateral hemifield and that distances in A1 and even R/RT were not categorically smaller. In other words, there exists spatial information in all cortical areas measured. This is underscored by the fact that receptive field shapes varied continuously within and across areas, as attempts to cluster and classify neurons had little success.

Both tuning area and tuning vector magnitude were correlated with BF, as might be expected due to the frequency dependence of the acoustic features that convey spatial information to the brain (Blauert 1997; Slee and Young 2010). We also found that neurons sampled in R/RT tended have low BF, which was associated with low spatial tuning selectivity, while neurons in CM/CL tended to have high BF, which was associated with high spatial tuning selectivity. Therefore, some of the differences in tuning selectivity between the three areas may be attributed to differences in frequency processing of the sampled populations. However, there were still differences (e.g., tuning vector magnitude for A1 versus R/RT, and tuning area for A1 versus CM/CL), which were still present when controlling for BF. Also, it may be the case that frequency maps are not identical across auditory cortical fields. Previous studies suggest that R and RT are biased toward low frequencies (Merzenich and Brugge

1973; Morel et al. 1993; Kosaki et al. 1997; Rauschecker et al. 1997; Recanzone et al. 2000; Bendor and Wang 2008), and CM and CL are biased toward high frequencies (Recanzone et al. 2000; Zhou and Wang 2012). Thus, to the extent that the representation of frequency is not equal between cortical areas, an inference can be made that spatial selectivity is still different between areas, even if such differences are smaller or nonexistent when controlling for frequency selectivity. A qualification of this argument is the fact that to our knowledge, no study has attempted to rigorously determine whether cochleotopic representation of R/RT and CM/CL is biased relative to A1 or each other, and the findings of previous studies may be influenced by the relative difficulty of sampling from cortical areas with high curvature, such as in sulci, particularly for marmosets (Bendor and Wang 2008).

To our knowledge, the interaction between frequency tuning and spatial selectivity has not been directly addressed in most previous works, although one study comparing spatial tuning across cortical areas reported no significant interaction between frequency tuning and spatial tuning width (Tian et al. 2001). A more recent study comparing spatial tuning in cats noted that neurons in the dorsal zone (DZ) tended to have higher BFs, although the authors speculated that this area is homologous to R in primates, as opposed to CM or CL (Lee and Middlebrooks 2013). A possible explanation for the positive correlation between BF tuning selectivity in the present full-field recordings could be that low BF neurons do not integrate frequency information within the range where the spectral cues differentiating locations in the median plane reside (Slee and Young 2010).

Implications for Coding and Decoding of Spatial Information

The results from the present study provide insight about how the entire space around a subject might be decoded from activity in auditory cortex. While there are no generally accepted models for encoding or decoding of spatial information carried by individual auditory cortex neurons, one proposed theory for azimuth coding is that the laterality of a sound source is represented by the relative firing strength of populations of neurons preferring either lateral pole (Stecker et al. 2005; Werner-Reiss and Groh 2008). However, this theory does not provide an account for how sound location is decoded throughout the full spatial field. The present results suggest an alternate hypothesis in which full-field tuning for each individual neuron is accounted for by the decoder. The fact that tuning vectors were biased toward contralateral locations and receptive fields were often oddly shaped or even multi-peaked would complicate the use of simple decoding schemes such as a labeled line code or a population vector (Georgopoulos et al. 1986). This constraint could be mitigated by not including "odd" neurons in the readout, but a more generalized decoder that does not make assumptions about receptive field shapes, such as log-likelihood decoder (Jazayeri and Movshon 2006), might serve as a potential candidate. In fact, such a decoder has been used to successfully decode azimuth in awake macaques (Miller and Recanzone 2009) and in the inferior colliculus of rabbits (Day and Delgutte 2013). Other decoding schemes based on temporal firing patterns have been applied to azimuth tuning in cats (Mickey and Middlebrooks 2003; Stecker et al. 2003; Lee and Middlebrooks 2013). Future work could address potential decoding strategies in the full spatial field.

Finally, the large number of narrow receptive fields observed in these cortical areas suggests that they are not the brain regions that maintain a stable percept in a dynamic spatial environment, whether due to self or source movement. Single-sound sources may be represented by completely non-overlapping neural populations within a single acoustic event; the visual system encounters a similar problem when making saccades to survey a visual scene (Melcher and Colby 2008). Understanding how the auditory system binds auditory objects in a changing and sometimes unpredictable spatial environment will require recording neural activity from free moving subjects. It is likely that many brain areas, including those involved in visual, motor, and vestibular processing, may be involved in accomplishing this task.

Authors' Contributions

E.D.R. and X.W. conceived and designed research. E.D.R. performed experiments and analyzed data. E.D.R. and X.W. interpreted results of experiments and wrote the manuscript.

Funding

This work was supported by National Institutes of Health Grant DC003180 (X.W.).

Notes

We thank J. Estes and N. Sotuyo for assistance with animal care; S. Slee, Y. Zhou, E. Young for valuable discussions on results; and M. Jeschke for contributing model illustrations of the recording setup. The present address of E.R. is McGovern Institute for Brain Research, Massachusetts Institute of Technology, Cambridge, MA 02139, USA. *Conflict of Interest*: None declared.

References

Aitkin LM, Merzenich MM, Irvine DR, Clarey JC, Nelson JE. 1986. Frequency representation in auditory cortex of the common marmoset (Callithrix jacchus jacchus). J Comp Neurol. 252: 175–185.

Barbour DL, Wang X. 2003. Auditory cortical responses elicited in awake primates by random spectrum stimuli. J Neurosci. 23:7194–7206.

Bendor D, Wang X. 2008. Neural response properties of primary, rostral, and rostrotemporal core fields in the auditory cortex of marmoset monkeys. J Neurophysiol. 100:888–906.

Benson DA, Hienz RD, Goldstein MH. 1981. Single-unit activity in the auditory cortex of monkeys actively localizing sound sources: spatial tuning and behavioral dependency. Brain Res. 219:249–267.

Bizley JK, Nodal FR, Parsons CH, King AJ. 2007. Role of auditory cortex in sound localization in the midsagittal plane. J Neurophysiol. 98:1763–1774.

Blauert J. 1997. Spatial hearing: the psychophysics of human sound localization. 3rd ed. Cambridge, MA: MIT Press.

Brugge JF, Reale RA, Hind JE. 1996. The structure of spatial receptive fields of neurons in primary auditory cortex of the cat. J Neurosci. 16:4420–4437.

Brugge J, Reale R, Hind J, Chan JC, Musicant AD, Poon PW. 1994. Simulation of free-field sound sources and its application to studies of cortical mechanisms of sound localization in the cat. Hear Res. 73:67–84.

Campbell RA, Schnupp JW, Shial A, King AJ. 2006. Binaural-level functions in ferret auditory cortex: evidence for a continuous

distribution of response properties. J Neurophysiol. 95: 3742–3755.
Day ML, Delgutte B. 2013. Decoding sound source location and separation using neural population activity patterns. J Neurosci. 33:15837–15847.
Eisenman LM. 1974. Neural encoding of sound location: an electrophysiological study in auditory cortex (A1) of the cat using free field stimuli. Brain Res. 75:203–214.
Fritz JB, Shamma S, Elhilali M, Klein D. 2003. Rapid task-related plasticity of spectrotemporal receptive fields in primary auditory cortex. Nat Neurosci. 6:1216–1223.
Furukawa S, Middlebrooks JC. 2002. Cortical representation of auditory space: information-bearing features of spike patterns. J Neurophysiol. 87:1749–1762.
Gaese BH, Ostwald J. 2001. Anesthesia changes frequency tuning of neurons in the rat primary auditory cortex. J Neurophysiol. 86:1062–1066.
Georgopoulos AP, Schwartz AB, Kettner RE, Schwartz AB. 1986. Neuronal population coding of movement direction. Science. 233:1416–1419.
Guo W, Chambers AR, Darrow KN, Hancock KE, Shinn-Cunningham BG, Polley DB. 2012. Robustness of cortical topography across fields, laminae, anesthetic states, and neurophysiological signal types. J Neurosci. 32:9159–9172.
Hackett TA. 2011. Information flow in the auditory cortical network. Hear Res. 271:133–146.
Jazayeri M, Movshon JA. 2006. Optimal representation of sensory information by neural populations. Nat Neurosci. 9: 690–696.
Jenkins WM, Masterton RB. 1982. Sound localization: effects of unilateral lesions in central auditory system. J Neurophysiol. 47:987–1016.
Kaas JH, Hackett TA. 1998. Subdivisions of auditory cortex and levels of processing in primates. Audiol Neurootol. 3:73–85.
Kaas JH, Hackett TA. 2000. Subdivisions of auditory cortex and processing streams in primates. Proc Natl Acad Sci USA. 97: 11793–11799.
Kadia SC, Wang X. 2003. Spectral integration in A1 of awake primates: neurons with single- and multipeaked tuning characteristics. J Neurophysiol. 89:1603–1622.
King AJ, Bajo VM, Bizley JK, Campbell P, Nodal FR, Schulz AL, Schnupp JWH. 2007. Physiological and behavioral studies of spatial coding in the auditory cortex. Hear Res. 229:106–115.
Kosaki H, Hashikawa T, He J, Jones EG. 1997. Tonotopic organization of auditory cortical fields delineated by parvalbumin immunoreactivity in macaque monkeys. J Comp Neurol. 386:304–316.
Lee C-C, Middlebrooks JC. 2011. Auditory cortex spatial sensitivity sharpens during task performance. Nat Neurosci. 14: 108–114.
Lee C-C, Middlebrooks JC. 2013. Specialization for sound localization in fields A1, DZ, and PAF of cat auditory cortex. J Assoc Res Otolaryngol. 14:61–82.
Lomber SG, Malhotra S. 2008. Double dissociation of "what" and "where" processing in auditory cortex. Nat Neurosci. 11: 609–616.
Lu T, Liang L, Wang X. 2001. Neural representations of temporally asymmetric stimuli in the auditory cortex of awake primates. J Neurophysiol. 85:2364–2380.
Makous JC, Middlebrooks JC. 1990. Two-dimensional sound localization by human listeners. J Acoust Soc Am. 87: 2188–2200.
Melcher D, Colby CL. 2008. Trans-saccadic perception. Trends Cogn Sci. 12:466–473.
Merzenich M, Brugge JF. 1973. Representation of the cochlear partition on the superior temporal plane of the macaque monkey. Brain Res. 50:275–296.
Mickey BJ, Middlebrooks JC. 2003. Representation of auditory space by cortical neurons in awake cats. J Neurosci. 23: 8649–8663.
Middlebrooks JC. 2014. Distributed cortical representation of sound locations. In: Popper AN, Fay RR, editors. Perspectives on auditory research. New York, NY: Springer. pp. 361–378.
Middlebrooks JC, Clock AE, Xu L, Green DM. 1994. A panoramic code for sound location by cortical neurons. Science. 264: 842–844.
Middlebrooks JC, Pettigrew JD. 1981. Functional classes of neurons in primary auditory cortex of the cat distinguished by sensitivity to sound location. J Neurosci. 1:107–120.
Middlebrooks J, Xu L, Eddins AC, Green DM. 1998. Codes for sound-source location in nontonotopic auditory cortex. J Neurophysiol. 80:863–881.
Miller LM, Recanzone GH. 2009. Populations of auditory cortical neurons can accurately encode acoustic space across stimulus intensity. Proc Natl Acad Sci USA. 106:5931–5935.
Morel A, Garraghty PE, Kaas JH. 1993. Tonotopic organization, architectonic fields, and connections of auditory cortex in macaque monkeys. J Comp Neurol. 335:437–459.
Mrsic-Flogel TD, King AJ, Schnupp JW. 2005. Encoding of virtual acoustic space stimuli by neurons in ferret primary auditory cortex. J Neurophysiol. 93:3489–3503.
Rajan R, Aitkin LM, Irvine DRF, Mckay J. 1990. Azimuthal sensitivity of neurons in primary auditory cortex of cats. I. Types of sensitivity and the effects of variations in stimulus parameters. J Neurophysiol. 64:872–887.
Rauschecker J. 1998. Parallel processing in the auditory cortex of primates. Audiol Neurootol. 3:86–103.
Rauschecker JP, Tian B. 2000. Mechanisms and streams for processing of "what" and "where" in auditory cortex. Proc Natl Acad Sci USA. 97:11800–11806.
Rauschecker JP, Tian B, Pons T, Mishkin M. 1997. Serial and parallel processing in rhesus monkey auditory cortex. J Comp Neurol. 382:89–103.
Razak KA, Yarrow S, Brewton D. 2015. Mechanisms of sound localization in two functionally distinct regions of the auditory. Cortex. 35:16105–16115.
Recanzone GH, Guard DC, Phan ML. 2000a. Frequency and intensity response properties of single neurons in the auditory cortex of the behaving macaque monkey. J Neurophysiol. 83:2315–2331.
Recanzone GH, Guard DC, Phan ML, Su TK. 2000b. Correlation between the activity of single auditory cortical neurons and sound-localization behavior in the macaque monkey. J Neurophysiol. 83:2723–2739.
Remington ED, Osmanski MS, Wang X. 2012. An operant conditioning method for studying auditory behaviors in Marmoset monkeys. PLoS One. 7:e47895.
Sadagopan S, Wang X. 2008. Level invariant representation of sounds by populations of neurons in primary auditory cortex. J Neurosci. 28:3415–3426.
Schnupp JW, Mrsic-Flogel TD, King AJ. 2001. Linear processing of spatial cues in primary auditory cortex. Nature. 414: 200–204.
Scott BH, Malone BJ, Semple MN. 2007. Effect of behavioral context on representation of a spatial cue in core auditory cortex of awake macaques. J Neurosci. 27:6489–6499.
Slee SJ, Young ED. 2010. Sound localization cues in the marmoset monkey. Hear Res. 260:96–108.

Slee SJ, Young ED. 2011. Information conveyed by inferior colliculus neurons about stimuli with aligned and misaligned sound localization cues. J Neurophysiol. 106:974–985.

Slee SJ, Young ED. 2013. Linear processing of interaural level difference underlies spatial tuning in the nucleus of the brachium of the inferior colliculus. J Neurosci. 33: 3891–3904.

Stecker GC, Harrington IA, Middlebrooks JC. 2005. Location coding by opponent neural populations in the auditory cortex. PLoS Biol. 3(3):e78.

Stecker GC, Mickey BJ, Macpherson EA, Middlebrooks JC. 2003. Spatial sensitivity in field PAF of cat auditory cortex. J Neurophysiol. 89:2889–2903.

Tian B, Reser D, Durham A, Kustov A, Rauschecker JP. 2001. Functional specialization in rhesus monkey auditory cortex. Science. 292:290–293.

Tibshirani R, Walther G, Hastie T. 2001. Estimating the number of clusters in a data set via the gap statistic. J R Stat Soc Series B Stat Methodol. 63:411–423.

Werner-Reiss U, Groh JM. 2008. A rate code for sound azimuth in monkey auditory cortex: implications for human neuroimaging studies. J Neurosci. 28:3747–3758.

Woods TM, Lopez SE, Long JH, Rahman JE, Recanzone GH. 2006. Effects of stimulus azimuth and intensity on the single-neuron activity in the auditory cortex of the alert macaque monkey. J Neurophysiol. 96:3323–3337.

Xu L, Furukawa S, Middlebrooks JC, Xu LI. 1998. Sensitivity to sound-source elevation in nontonotopic auditory cortex. J Neurophysiol. 80:882–894.

Yao JD, Bremen P, Middlebrooks JC. 2013. Rat primary auditory cortex is tuned exclusively to the contralateral hemifield. J Neurophysiol. 110:2140–2151.

Yu JJ, Young ED. 2000. Linear and nonlinear pathways of spectral information transmission in the cochlear nucleus. Proc Natl Acad Sci USA. 97:11780–11786.

Zhou B, Green DM, Middlebrooks JC. 1992. Characterization of external ear impulse responses using Golay codes. J Acoust Soc Am. 92:1169–1171.

Zhou Y, Wang X. 2012. Level dependence of spatial processing in the primate auditory cortex. J Neurophysiol. 108:810–826.

Zurita P, Villa AEP, de Ribaupierre Y, de Ribaupierre F, Rouiller EM. 1994. Changes of single unit activity in the cat's auditory thalamus and cortex associated to different anesthetic conditions. Neurosci Res. 19:303–316.